Technium Vol. 31, pp.9-45 (2026)
ISSN: 2668-778X
www.techniumscience.com

Sustainable nanophysics: Green synthesis production of magnesium oxide nanostructures for advanced biological activity

Diyaa Y. Hussein[1]

[1]Department of physics, College Science, University of Sumer, Iraq

* Corresponding author. E-mail addresses: Physicsdisr@gmail.com

Graphical abstract

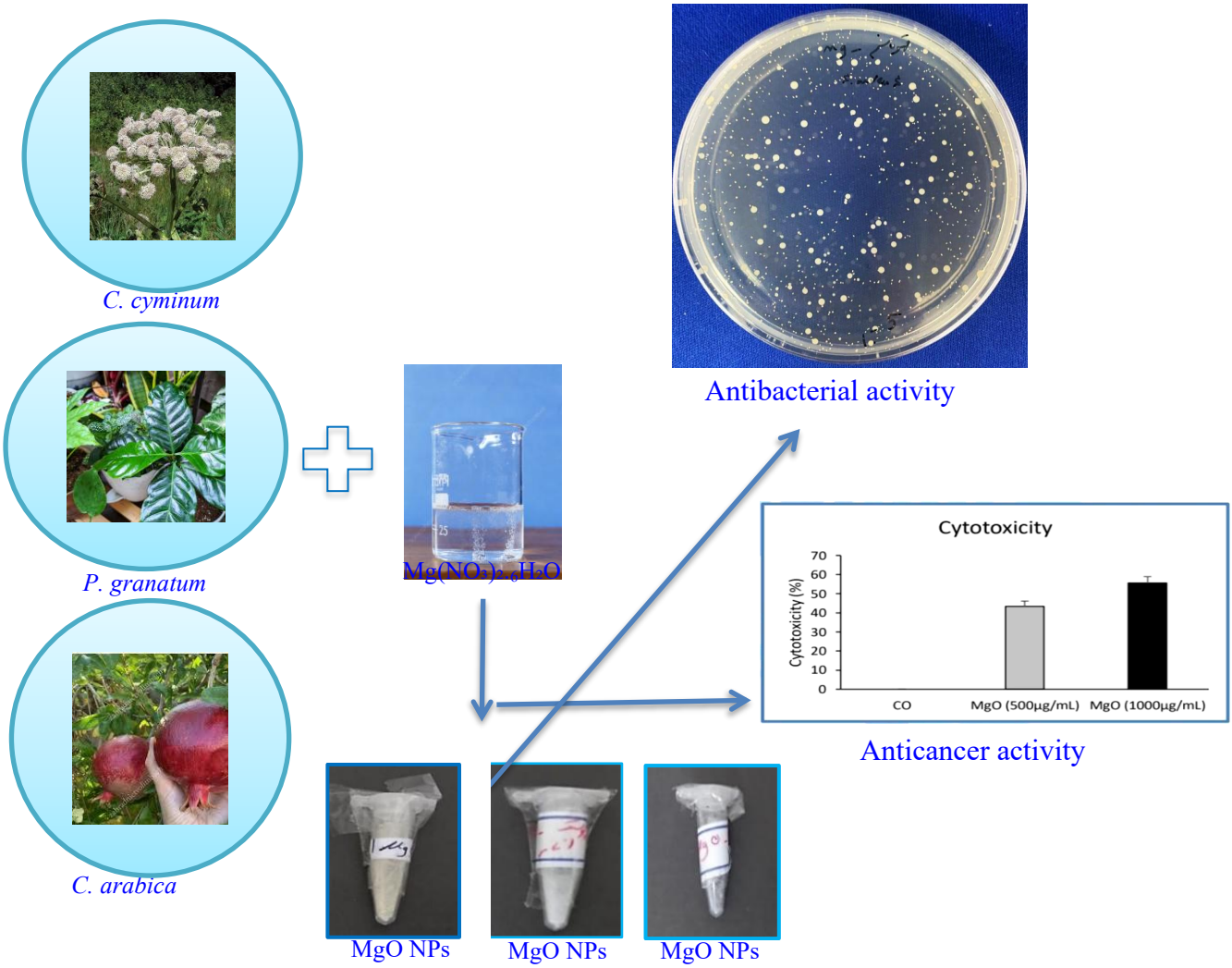

Technium Vol. 31, pp.9-45 (2026)
ISSN: 2668-778X
www.techniumscience.com

Abstract

In this work, a novel green synthesis for producing magnesium oxide nanoparticles (MgO NPs) using three plant extracts— *cumin (C. cyminum), pomegranate (P. granatum),* and *coffee (C. arabica)*—for sustainable nanophysics and demonstrating enhanced antibacterial activity against Staphylococcus aureus (S. aureus) and Escherichia coli (E. coli) and anticancer activity against cervical cancer cells. MgO NPs was characterized by XRD patterns, FESEM images, EDX analysis, FTIR spectrum, and UV-visible spectrum to study the nanophysics (structure and optical) properties. The average crystalline sizes and nanocrystals of MgO NPs prepared using *(C. cyminum), (P. granatum),* and *(C. arabica)* extracts were (21.26, 21.39, and 18.32) nm with face-centered cubic (FCC), respectively, as confirmed using XRD patterns. FE-SEM showed the morphology and the particle size of MgO NPs prepared using these extracts indicated mostly spherical and irregularly nanoparticles shaped with (24.95, 19.68, and 13.89) nm, respectively, while EDX analysis confirmed the high purity of Mg and O elements. The FTIR spectrum confirmed the strong absorption peak of MgO NPs prepared using (*C. cyminum*), (*P. granatum*), and (*C. arabica*) extracts were 414 to 646 cm^{-1}, 418 to 648 cm^{-1}, and 419 to 649 cm^{-1}, respectively, by revealing unique Mg–O stretching vibrations. The energy band gaps of MgO NPs prepared using (*C. cyminum), (P. granatum),* and *(C. arabica)* extracts were 5.7 eV, 5.9 eV, and 5.8 eV, respectively, as revealed by UV-Vis spectrum. According to this study, gram-positive bacteria (S. aureus) had inhibitory zones of 99.98%, 99.50%, and 68.39%, respectively. The inhibition ratios of gram-negative bacteria (E. coli) were 82.22%, 71.87%, and 68.75%, respectively. Additionally, at a dosage of 1000 µg/mL, MgO NPs prepared using (*C. cyminum) extract* showed 55.57% cell death against cervical cancer cells (HeLa line), indicating strong anticancer potential.

Key-words: MgO NPs; Green synthesis; plant extract; antibacterial activity; cervical cancer cells.

1. Introduction

Nanotechnology represents a rapidly evolving frontier in scientific research, offering revolutionary advances across a wide range of fields [1-5]. Among various NPs, MgO NPs have attracted considerable attention due to their exceptional chemical stability, high surface area, and notable biological properties [6-10]. MgO NPs possess unique optical, mechanical,

and antibacterial characteristics, making them highly desirable for applications in environmental, biomedical, and optical devices [11-15]. Traditional chemical and physical synthesis methods for producing NPs often involve toxic reagents and energy-intensive processes [16-18]. As an alternative, green synthesis has emerged as an eco-friendly and cost-effective route, utilizing biological resources such as plant extracts (*C. cyminum, P. granatum, and C. arabica*) to mediate the formation of NPs [19-21]. Plant-mediated synthesis not only eliminates the need for hazardous chemicals but also offers natural capping and stabilizing agents, enhancing the biocompatibility and functionality of the resulting NPs [22-25]. This study focuses on the green synthesis of MgO NPs using (*C. cyminum, P. granatum, and C. arabica)* extracts—all rich in photochemicals capable of reducing and stabilizing metal ions [26-29]. Today, diverse plant sources are employed to synthesize green NPs. Plant seed and leaf extracts are useful stabilizers for the synthesis of biogenetic NPs, according to researchers. The biological activities of green NPs are precisely determined by the plant types from which the extracts are derived, as well as the abundance of antimicrobial/anti-carcinogenic chemicals found in the plant [30].

C. cyminum, a medicinally significant plant high in flavonoids, phenolics, and terpenoids, is ideal for green synthesis due to its bioactive features [31]. *C. cyminum* extract not only speeds up the formation of NPs, but it also improves their biological activity [32-33].

Pomegranate fruit is considered healthy for the human diet. In the *P. granatum* juice industry, the peel of a *P. granatum* accounts for around 50% of its weight and is a rich source of polyphonic compounds. *P. granatum* have been used to cure a variety of human ailments, including diarrhea, vomiting, headaches, colitis, dysentery, and ulcers. *P. granatum* extract offers a wide range of biological activities, including antioxidant, anti-inflammatory, and anti-carcinogenic qualities; it is used to treat cancer, tooth infections, and bacterial wounds. *P. granatum* extract contains bioactive compounds that are known to have antioxidant and antibacterial activities [34].

Global *C. arabica* production surpasses 168 million metric tons per year, with coffee husk accounting for 30-50% of the entire yield. *C. arabica* husk, which was formerly discarded or utilized as a low-value fertilizer, is now recognized as a valuable material for green NP synthesis. Recent research has shown that spent *coffee* ground extracts and *C. arabica seed* extracts are useful in the production of silver NPs, particularly in terms of physiochemical qualities and biological applications. However, research into the utilization of *C. arabica* husk as a sustainable precursor for NP production is still limited [35].

When compared to the current chemical approaches, plant-mediated synthesis is the preferable biosynthesis source due to its less biohazardous environment, reduced energy consumption, easy/promising scaling up, and simply less purification required [36-38].

In the literature, some studies have been conducted on green NPs synthesized from *Cuminum cyminum L. (C. cyminum)* extract to investigate their biological properties. *C. cyminum* is the most common spice used in Asian cuisine products. *C. cyminum* oil's principal components include cuminaldehyde, cymene, and terpenoids [39]. Some researchers have established that some of the key active components in cumin oil, such as cuminal and chimeric alcohol, displayed very high anti-cancer effects on colon and lung malignancies [40]. In 2022, synthesis of iron oxide NPs using the *henna leaves* extract for anticancer activity by Duha A. Kadhim [41]. In 2022, iron oxide NPs using *chili* extract with iron rust for antibacterial activity were developed by Muslim A. Abid and Duha A. Kadhim [42]. Copper oxide NPs were synthesized using the *blood* extract for antibacterial activity by Duha A. Kadhim [43]. AgO NPs, MnO NPs, and AgO/MnO NPs were synthesized from the *Malva* extract for antibacterial activity by Muslim A. Abid [44]. In 2025, synthesis of SnO_2 NPs using the *Croton malabaricus bedd* extract for antioxidant, antibacterial activity, and anti-biofilm by Nayan Kumar Sishu et al. [45]. In 2025, ZnO NPs were prepared using the plant extract (*Cichorium intybus L. root*) for biomedical applications via Nayan Kumar Sishu et al. [46]. In 2025, Au-ZnO nanocomposite was synthesized using *plant* extract for photocatalytic activity of MB dye by Arunadiri Sharmila et al. [47]. In 2025, the in silico test demonstrated how well the phytocompounds might attach to the protein targets that fight cancer, diabetes, and germs via Nayan Kumar Sishu et al. [48].

The green synthesis approach is regarded as more cost-effective than standard chemical procedures since it uses natural plant extracts such as *C. cyminum leafs, P. granatum peels, and C. arabica seeds* while avoiding expensive chemical processes. Compared to traditional synthesis, green synthesis offers a 30% decrease in energy usage, up to 40% cost savings, and a 50% increase in industrial output. Antibacterial, anticancer agents, antioxidants, and drug delivery methods are all examples of biomedical uses. Carbon quantum dots and photovoltaic are covered under the energy section. The agricultural and food industries prioritize nano fertilization, insect control, and food quality. Environmental remediation includes the cleaning of water and soil by Ahmed I. Osman [49].

In this work, three distinct plant extracts—*C. cyminum, P. granatum, and C. arabica*—were used to create MgO NPs in an environmentally friendly manner. The nanophysics (structural, chemical, and optical) characteristics of the produced MgO NPs were assessed using a comprehensive characterization process that included XRD patterns, FTIR spectrum, FE-SEM images, EDX analysis, and UV-Vis spectroscopy. In addition to characterization, the MgO NPs antibacterial effectiveness was evaluated against both Gram-positive and Gram-negative bacteria, and their anticancer potential against cervical cancer cell lines was also evaluated. The use of integrated multi-plant extracts in green synthesis to improve biological activity and environmental safety has not received much attention, despite the large number of studies on MgO NPs. By offering a sustainable and environmentally friendly synthesis technique that makes use of the synergistic potential of several phytochemicals, our study seeks

to close this gap. The study also highlights the environmental and biological significance of MgO NPs, emphasizing their potential uses in antibacterial and anticancer therapies.

2. Experimental work

2.1 Materials and Methods

Magnesium nitrate [$Mg(NO_3)_{2.6}H_2O$, ≥98% purity, ACS grade] was purchased from Sigma-Aldrich (China). Plants (*C. cyminum, P. granatum*, and *C. arabica*) were purchased from a local market in Baghdad, Iraq. The apparatus and materials applied in this work include an oven (SRJX-5-13 model box—resistance furnace control box), a magnetic stirrer (Rlabinco, Lebanon), and an electronic balance (Sartorius, Germany).

2.2 Green synthesis of plant (*C. cyminum, P. granatum*, and *C. arabica*) extracts

The *C. cyminum, P. granatum*, and *C. arabica* were thoroughly washed with deionized water to remove any surface impurities, followed by careful removal of internal organs. The cleaned specimen was then dried using a traditional clay oven to ensure complete moisture removal and subsequently ground manually using a mortar and pestle to obtain a fine powder. 10 g of *C. cyminum, P. granatum*, and *C. arabica* were placed into a glass beaker containing 100 mL of deionized water, respectively. The mixtures were homogenized using a magnetic stirrer at a constant temperature of 70°C for two hours. Upon completion of the reaction, the solution was filtered using Whatman filter paper to remove large particulates; the filtration process was repeated several times to ensure purity. The resulting filtrate was stored in airtight glass containers for subsequent use in the preparation of MgO NPs. Muslim A. Abid calculated the extraction yield by drying a certain volume of the filtrate and weighing the amount of solid material that was left behind [50–51]. The corresponding extraction yields for (*C. cyminum , P. granatum*, and *C. arabica*) were 6.4%, 8.5%, and 10.3%, respectively.

2.3 Green synthesis of MgO NPs using plant (*C. cyminum, P. granatum*, and *C. arabica*) extracts

Synthesis of MgO NPs via green methods using three plant (*C. cyminum, P. granatum*, and *C. arabica*) extracts. In each synthesis, 100 mL of the plant (*C. cyminum, P. granatum*, and *C. arabica*) extracts were mixed with 10.4 g of magnesium nitrate hexahydrate ($Mg(NO_3)_2 \cdot 6H_2O$) dissolved in 100 mL of distilled water at 70–80°C. MgO NPs were synthesized from *C. cyminum, P. granatum,* and *C. arabica* extracts, which served as natural sources of reducing and stabilizing agents, using a plant-mediated green synthesis approach. MgO NPs that were phase-pure were obtained after two hours of calcination at 500°C. Following impurity removal and drying, the final products displayed clear color variations based on the plant source, ranging from light sand to dark gray, representing variations in

particle properties driven by the photochemical makeup of each extract [52]. A schematic overview of the synthesis protocol is depicted in Figure 1 A-C.

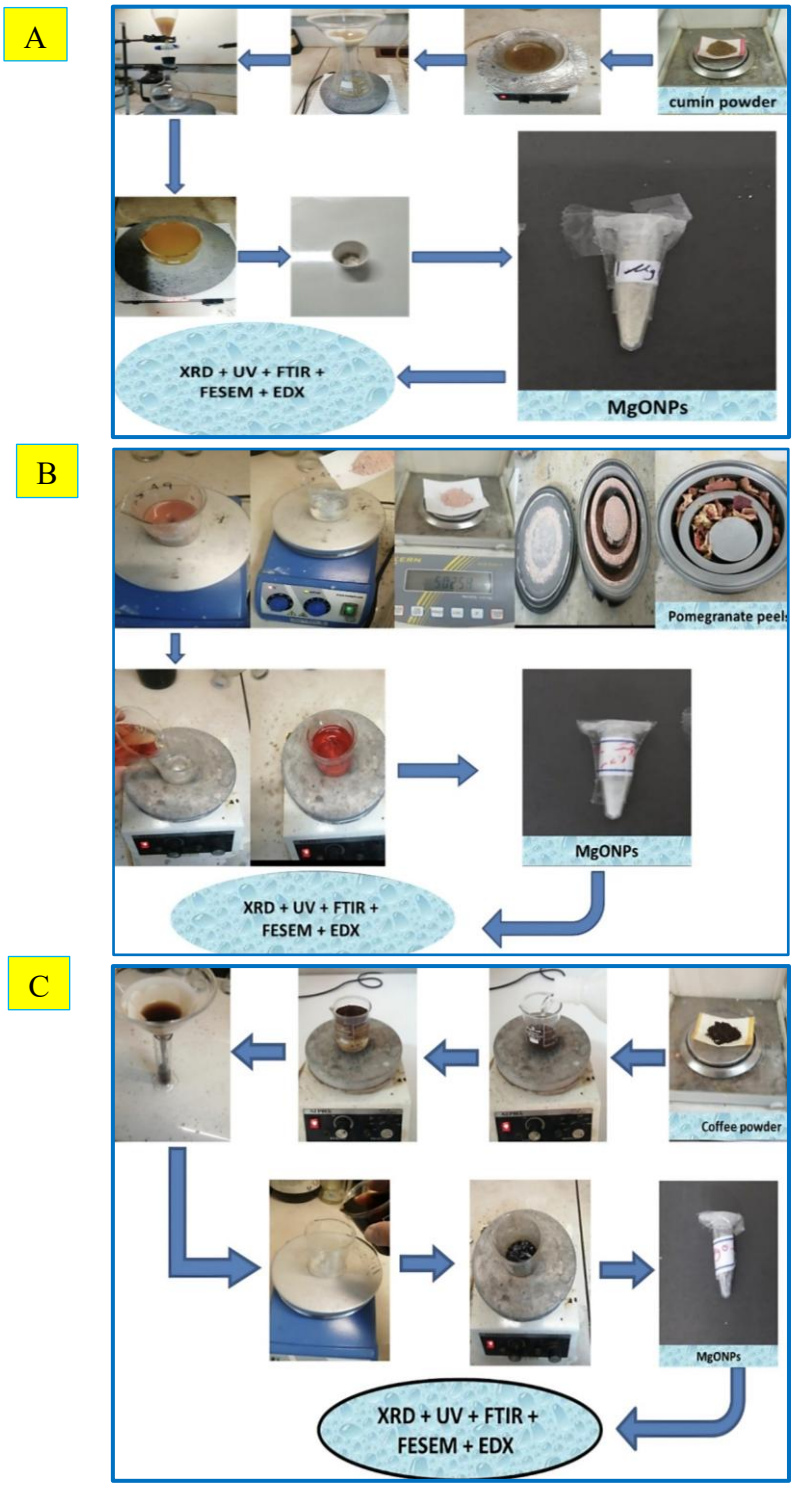

Figure 1: Schematic illustration of the green synthesis process of MgO NPs, (A) *C. cyminum* extract, (B) *P. granatum* extract, and (C) *C. arabica* extract.

2.4 Antibacterial activity of MgO NPs using plant (*C. cyminum, P. granatum,* and *C. arabica*) extracts

This study uses two different types of bacteria strains: Gram-positive Staphylococcus aureus ATTC25923 and Gram-negative Escherichia coli ATTC25922. Escherichia coli is a gram-negative, facultative anaerobe. Staphylococcus aureus, a Gram-positive bacterium, is spherically shaped and belongs to the Bacillota. They are commonly seen in the upper respiratory tract and on the epidermis. The genus Staphylococcus has more than 40 species, including Staphylococcus, a Gram-positive bacterium. E. coli are coli form germs that do not form spores. Rod-shaped cells are the norm. It has been associated with pneumonia in patients with diabetes or alcohol use disorders, and it is found in the environment. The microbial cultures were provided by the Microbiology Laboratory at the University of Mustansiriyah-College of Science. This test was carried out utilizing the agar-well diffusion approach, which involved using sterile nutritional agar as the medium in sterile petri dishes of 90 mm in diameter. The nutritional agar medium was made by dissolving 0.6 g of peptone (organic nitrogen), 0.4 g of yeast extract (vitamins, carbs, nitrogen, and minerals), and 28 g of agar (firmness) in 1000 mL of distilled water. At a temperature of 28°C, the pH was set to 6.9. To ensure that the components are fully blended, they are combined and heated to 121°C for around 15 minutes. The MgO NPs were then dissolved in a 30 mg/mL solution of Baseline (control). Recently created bacteria were placed on the petri dish's surface. A sterile gel puncher/cork borer was used to create 8 mm diameter wells in the bacterial medium of each plate. For microorganisms, each well contains 40 µL of MgO NPs, and the appropriate quantity of Baseline (control). The inhibitory zone was determined in millimeters after incubating test samples at ±25°C for 24 hours to stimulate bacterial growth. The inhibitory zone was determined in millimeters after incubating test materials at ±25°C for 24 hours to stimulate bacterial growth. $Mn(NO_3)_2$ salt is mixed with *C. cyminum, P. granatum,* and *C. arabica* extracts to create MgO NPs. These substances help to prevent two types of bacteria, all of which have the potential to cause a variety of human disorders. The bacterial cell wall's adhesion and penetration eventually cause the cell's death, as demonstrated by structural changes to the cell membrane, such as increased permeability. They have now been identified as promising antibacterial agents capable of targeting both intracellular and extracellular sites [53]. The inhibition zone percentages are ascertained by employing the subsequent equation:

$$Inhibition\ Zone\ (\%) = \frac{Diameter\ of\ the\ inhibition\ zone\ in\ mm}{Diameter\ of\ pertiplate\ (90\ mm)} \text{x}\ 100\% \quad (1)$$

2.5 Anticancer activity cell line (Hela) of MgO NPs using plant (*C. cyminum, P. granatum,* and *C. arabica*) extracts

Cancer cells line (Hela) (acquired from the American Type Culture Collection in Manassas, Virginia). Cells were grown in high glucose Dulbecco's modified Eagle's medium (Gibco Laboratories, Grand Island, NY, USA) with 10% heat-inactivated fetal bovine serum, 100 units/mL penicillin, and 100 µg/mL streptomycin (Invitrogen, Carlsbad, CA) at 37°C in a 5% CO_2 humidified environment. The medium was replaced every two days during the incubation period. After reaching

70-80% confluence, cells were starved to induce quiescence before being treated with the experimental reagent.

2.6 Cell viability assay of MgO NPs using plant (*C. cyminum, P. granatum,* and *C. arabica*)

Cell viability was determined using a colorimetric test technique (XTT Cell Proliferation Kit). RAW 264.7 Hela cells (2 × 105 cells/well) were seeded in 96-well plates and incubated at 37°C in a humidified 5% CO_2/95% air environment for 48 hours. Cells were treated with 500 µg/ml and 1000 µg/ml of MgO NPs, and 500 µg/ml of CO for 48 hours. XTT solution (50 µL) was added to each well, incubated for 4 hours, and absorbance was measured at 450 nm with a reference wavelength at 670 nm using a microplate reader (Molecular Devices, Sunnyvale, CA).

2.7 Characterization of MgO NPs using plant (*C. cyminum, P. granatum,* and *C. arabica*) extracts

The Joint Committee on Powder Diffraction Standards (JCPDS) XRD was used to identify the MgO NPs phases with *C. cyminum, P. granatum,* and *C. arabica* extracts using CuKα radiation (1.5418 Å) as the source. It collected intensity data from 20° to 80° in step scan mode (XRD-6000). XRD measurements were used to study the phase analysis of MgO NPs produced in the Nanotechnology Laboratory and Advanced Materials Department of the Ministry of Science and Technology in Iraq. "A FE-SEM (JAEL JSM-6460LV)" has been used to determine the shape and particle size of MgO NPs using FE-SEM. The FE-SEM field provided information about the tiny structure and size of particles, along with their shapes, at different zoom levels using a voltage of 20.00 kilovolts (KV). The Fourier transformed infrared spectrum (FTIR) from the Spectrum GX FT-IR, made by Perkin-Elmer, which has a potassium bromide (KBr) beam splitter and a mid-IR triglycine sulfate (TGC) detector, to analyze the functional groups and vibration modes through polarized IR reflectance. The energy band gap measured was determined by analyzing the UV-visible spectra from the SHAMIZDA-1800UV spectrometer [54].

2.8 Role and mechanism of MgO NPs using plant (*C. cyminum, P. granatum,* and *C. arabica*) extracts

The green synthesis of MgO NPs seeks to reduce the usage of harmful chemicals by using bioactive molecules derived from plant extracts as reducing and stabilizing agents. These extracts can be derived from many parts of the plant, such as leaves, seeds, flowers, stems, bark, roots, or even the entire plant [55]. In recent years, a wide range of plant species have been employed in the green synthesis of MgO NPs, demonstrating the versatility of plant-based methods. MgO NPs are created using plant (*C. cyminum, P. granatum, and C. arabica*) extracts by using natural substances in the bioreactor to convert Mg^{2+} ions into a different form, such as uric acid, amino acids, and reducing sugars. Nanoscale nuclei are formed at the start of the process. Particles slowly grow, and cuminaldehyde (major volatile oil), limonene, β-pinene, flavonoids (apigenin, luteolin), phenolic acids (caffeic, ferulic), ellagic acid, punicalagin, gallic acid, catechins, flavonols (quercetin, kaempferol), and tannins Caffeine, chlorogenic acids (CGA), trigonelline, cafestol, kahweol, and

melanoidins stabilize the surface. $Mg(NO_3)_2$ salt, which is the main product of reduction, is then changed into MgO NPs through oxygen oxidation or heat treatment. This technique makes stable MgO NPs. Phenolic acid is an electron-rich substance that is an effective $Mg(NO_3)_2$ reducer and is the primary component of *C. cyminum, P. granatum, and C. arabica*, responsible for the crystalline of *C. cyminum, P. granatum, and C. arabica*, as shown in table 1. FT-IR analysis has revealed the presence of groups of functional compounds that react with and reduce metal ions [56].

$$Mg(NO_3)_2 + C.\ cyminum \text{ extract} \longrightarrow MgO + H_2O + NO^{-2} \longrightarrow \text{MgO NPs} \quad (2)$$

$$Mg(NO_3)_2 + P.\ granatum \text{ extract} \longrightarrow MgO + H_2O + NO^{-2} \longrightarrow \text{MgO NPs} \quad (3)$$

$$Mg(NO_3)_2 + C.\ arabica \text{ extract} \longrightarrow MgO + H_2O + NO^{-2} \longrightarrow \text{MgO NPs} \quad (4)$$

Table 1: Bioactive substances for *C. cyminum , P. granatum,* and *C. arabica* extracts.

Plant Material	Key Bioactive Compounds	Biological Activities / Functions
Cumin (C. cyminum)	Cuminaldehyde (major volatile oil), Limonene, β-Pinene, Flavonoids (apigenin, luteolin), Phenolic acids (caffeic, ferulic)	Antioxidant, Antibacterial, Anti-inflammatory, Hypoglycemic
Pomegranate Peels (P. granatum)	Ellagic acid, Punicalagin, Gallic acid, Catechins, Flavonols (quercetin, kaempferol), Tannins	Strong antioxidant, Anticancer, Antibacterial, Chelating agent in nanoparticle synthesis
Coffee (C. arabica)	Caffeine, Chlorogenic acids (CGA), Trigonelline, Cafestol, Kahweol, Melanoidins	Antioxidant, CNS stimulant, Hepatoprotective, Antimicrobial, Antidiabetic

3. Structural Properties

3.1 X-Ray diffraction of MgO NPs using plant (*C. cyminum, P. granatum,* and *C. arabica*) extracts

The X-ray diffraction (XRD) patterns of MgO NPs synthesized by green methods using (*C. cyminum, P. granatum,* and *C. arabica*) extracts revealed well-defined peaks corresponding to the cubic phase of MgO, with no evidence of impurities or secondary phases—indicating high sample purity. The diffraction peaks matched the standard JCPDS cards (00-045-0946 for MgO), confirming a face-centered cubic (FCC) structure with equal and orthogonal crystal axes ($a = b = c = 4.21$ Å; $\alpha = \beta = \gamma = 90°$). Prominent diffraction peaks were observed at approximately 36.8°, 42.9°, 62.2°, 74.5°, and 78.5°, corresponding to the (111), (200), (220), (311), and (222) planes, respectively; this result is consistent with a reference [57]. As shown in figure 2, the average crystalline sizes of MgO NPs using *C. cyminum, P. granatum, and C. arabica* were 21.264 nm, 21.394 nm, and 18.32 nm, respectively. Additional parameters such as dislocation density and micro-strain were also evaluated and summarized in Tables 2 and 3. The findings in Table 3 show that the MgO NPs prepared using three plant-based samples under investigation—*C. cyminum, P. granatum, and C. arabica*—show notable differences in average crystallized size, dislocation density, and micro-strain. Interestingly, the shortest average crystalline size of MgO NPs was

prepared using *C. cyminum* (18.322 nm), whereas *P. granatum* (21.394 nm) and *C. arabica* (21.264 nm) had the largest. This reduction in crystal size is associated with the maximum dislocation density and micro-strain values of any sample, which are found in *C. arabica*. The inherent chemical makeup and the thermal treatment parameters used during sample preparation are responsible for these findings. *C. arabica* probably experiences non-uniform nucleation and fast crystallization, producing smaller, defect-rich crystalline since it includes complex organic compounds like lipids and polyphenols. On the other hand, the creation of larger and more organized crystalline is supported by *C. cyminum* and *P. granatum*, which contain more chemically stable substances. The observed patterns are explained by the inverse relationship between crystalline size and dislocation density, which is in line with the theoretical relation δ = 1 / D^2. Additionally, there is a clear correlation between the rise in micro-strain and the increase in dislocation density, suggesting that a higher concentration of structural defects leads to enhanced lattice distortions. These results highlight the crucial role that synthesis circumstances and raw material composition play in determining the nanostructure and defect-related characteristics of bio-derived nanomaterials. The average crystal size calculated using the Scherrer equation as follows:

$$D\ (C.\ S.) = \frac{0.9\lambda}{\beta\cos\theta} \tag{5}$$

Where D is the crystalline size (nm), k is the shape factor, λ is the wavelength, β is the full width at half maximum, and θ is the angle of peak.

The dislocation density is calculated by this equation [58]:

$$\delta = 1/D^2\ (\text{Line}^2/\text{m}^2) \times 10^{15} \tag{6}$$

Where δ is the dislocation density were estimated using this equation [58]:

$$\varepsilon = \beta \cos\theta/4 \tag{7}$$

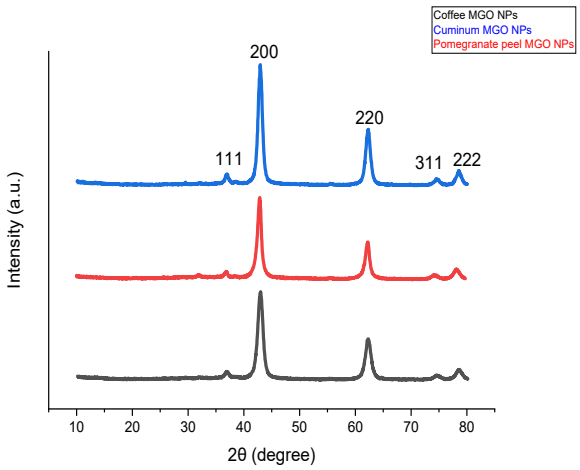

Figure 2: XRD patterns of MgO NPs synthesized using *C. cyminum, P. granatum, and C. arabica* extracts.

Table 2: XRD patterns of MgO using *C. cyminum, P. granatum, and C. arabica* extracts by green synthesis.

Sample type	Pos. [°2Th.]	FWHM [°2Th]	d-spacing [Å].	D (nm) crystalline (size)	(*hkl*)
C. Cuminum	36.770	0.620	2.44205	16.70	*(111)*
	42.759	0.807	2.11307	14.00	*(200)*
	62.124	0.860	1.49293	20.62	*(220)*
	74.220	1.400	1.27137	21.75	*(311)*
	78.330	1.230	1.21691	33.25	*(222)*
P. Granatum	36.944	0.820	2.43121	12.63	*(111)*
	42.912	0.904	2.10588	13.17	*(200)*
	62.241	1.012	1.49041	17.65	*(220)*
	74.560	1.170	1.27173	27.32	*(311)*
	78.538	1.160	1.21698	36.20	*(222)*
C. arabica	36.970	0.950	2.42976	10.93	*(111)*
	42.932	1.097	2.10492	10.33	*(200)*
	62.272	1.160	1.48973	15.36	*(220)*
	74.610	1.360	1.27102	22.94	*(311)*
	78.550	1.300	1.21684	32.05	*(222)*

Table 3: The average crystalline size values, the dislocations density, and the micro-strain of the MgO NPs using *C. cyminum, P. granatum, and C. arabica* extracts.

Sample type	Average crystalline size (nm)	dislocations density (δ*10^{-3} nm^{-2})	Microstrains *$10^{-3}\varepsilon$
C. Cuminum	21.264	3.5	3.970653358
		5.1	4.177047053
		2.3	2.178401547
		2.1	1.896875934
		0.9	1.219251664
P. granatum	21.394	6.2	5.218394862
		5.7	4.654137713
		3.2	2.550785653
		1.3	1.549454388
		0.7	1.128884596

C. arabica	18.322	8.3	3.970653358
		9.3	4.177047053
		4.2	2.178401547
		1.9	1.896875934
		0.9	1.219251664

3.2 FE-SEM and EDX of MgO NPs using plant (*C. cyminum, P. granatum,* and *C. arabica*) extracts

FE-SEM analysis revealed that the morphology and size of MgO NPs varied significantly depending on the type of plant extract used in the green synthesis process. The morphology and the average particle size of MgO NPs synthesized using the *C. cyminum, P. granatum*, and *C. arabica* extracts resulted in irregularly shaped particles, ranging from spherical to hexagonal forms, with large aggregates being 24.95 nm in size for MgO NPs using the *C. cyminum* extract, as shown in figure 3 (a-b). In contrast, as shown in Figure 4 (a-b), MgO NPs synthesized using the *p. granatum* extract produced smaller particles size (approximately 19.68 nm) with irregular surfaces. As shown in Figure 5 (a-b), MgO NPs prepared using the *C. arabica* extract yielded the smallest and most uniform particles (approximately 13.89 nm), exhibiting regular spherical and hexagonal morphology.

These differences are attributed to the specific phytochemical composition of each extract, particularly their content of bioactive compounds such as phenolics, flavonoids, proteins, and sugars. These compounds play critical roles in the reduction of Mg^{2+} ions and stabilization of NPs during synthesis. The high phenolic and flavonoid content in *C. arabica* extract likely contributed to the formation of smaller, more regularly shaped crystals. In contrast, the proteins and sugars in *C. cyminum* extract may have interfered with crystal growth, leading to the formation of irregular aggregates.

Figures 3, 4, and 5 (c-d) reveal EDX analysis, which confirmed the presence of magnesium (57.58, 54.52, and 56.30%) and oxygen (42.42, 45.18, and 43.70%) in ratios close to the stoichiometric composition of MgO NPs using *C. cyminum, P. granatum, and C. arabica*, respectively, indicating high purity and successful synthesis. While experimental conditions such as the reaction temperature (500°C) and time promoted crystallization, they were not the primary factors influencing NPs characteristics. Therefore, the chemical diversity of plant extracts can be strategically utilized to tailor the properties of MgO NPs for diverse medical, environmental, and electronic applications [59-61].

Technium Vol. 31, pp.9-45 (2026)
ISSN: 2668-778X
www.techniumscience.com

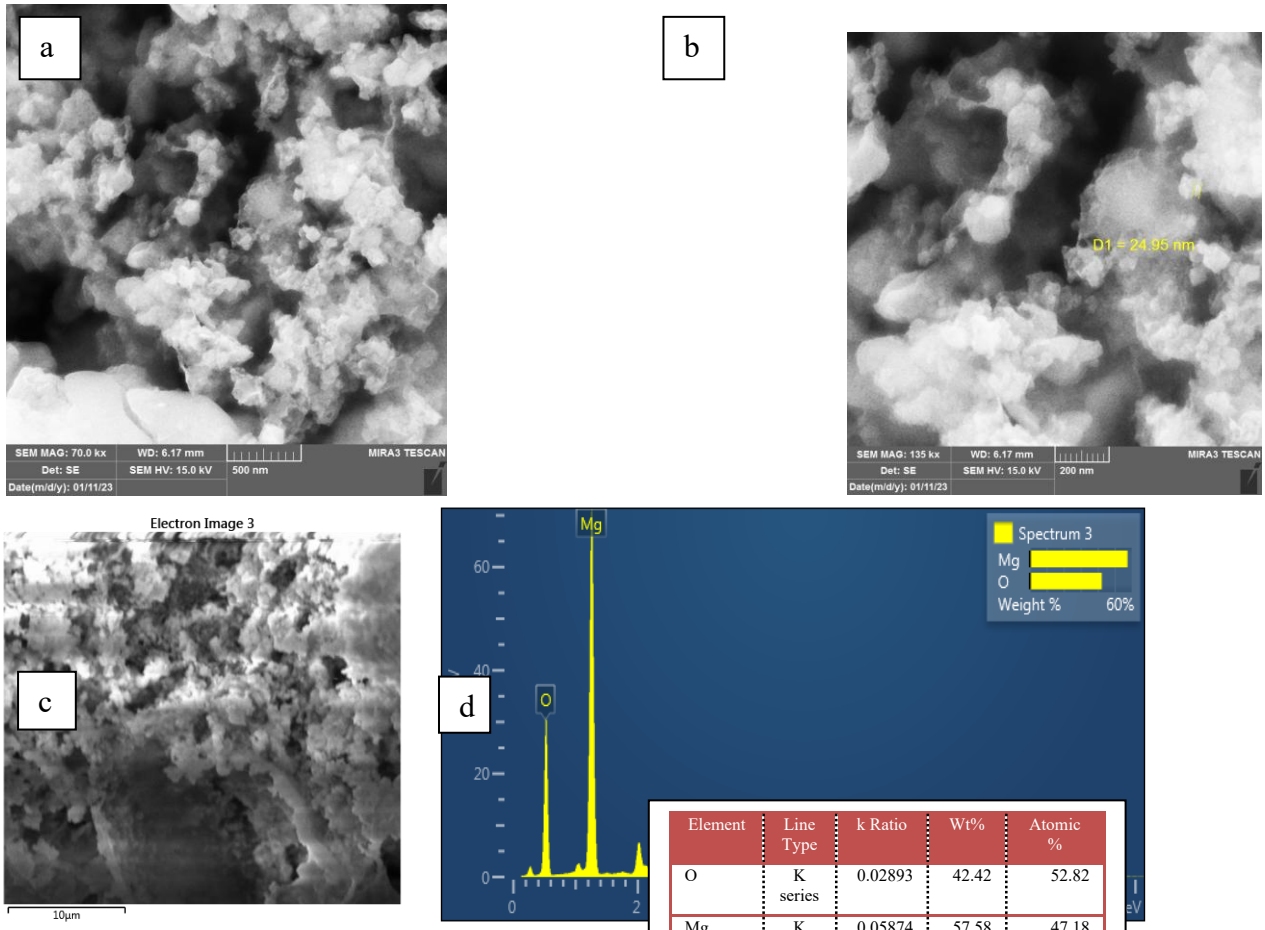

Element	Line Type	k Ratio	Wt%	Atomic %
O	K series	0.02893	42.42	52.82
Mg	K series	0.05874	57.58	47.18

Figure 3: FE-SEM morphological images and EDX elemental characterization of MgO NPs synthesized using the *C. cyminum* extract.

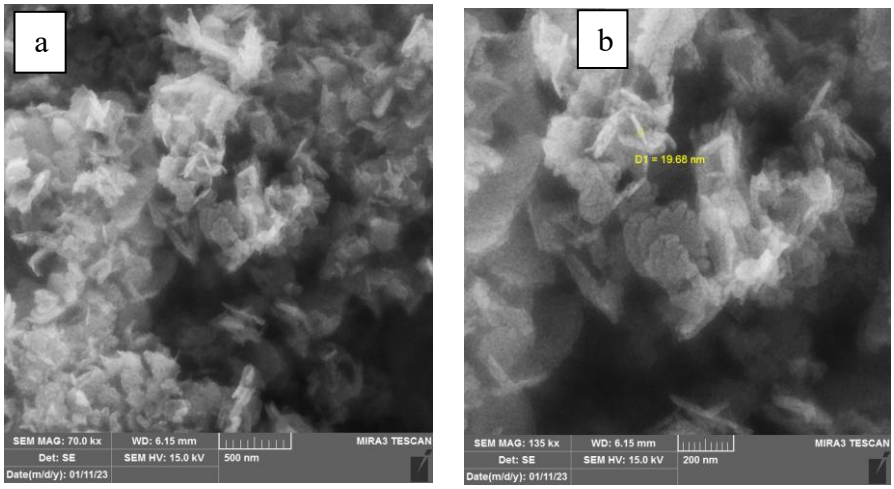

Technium Vol. 31, pp.9-45 (2026)
ISSN: 2668-778X
www.techniumscience.com

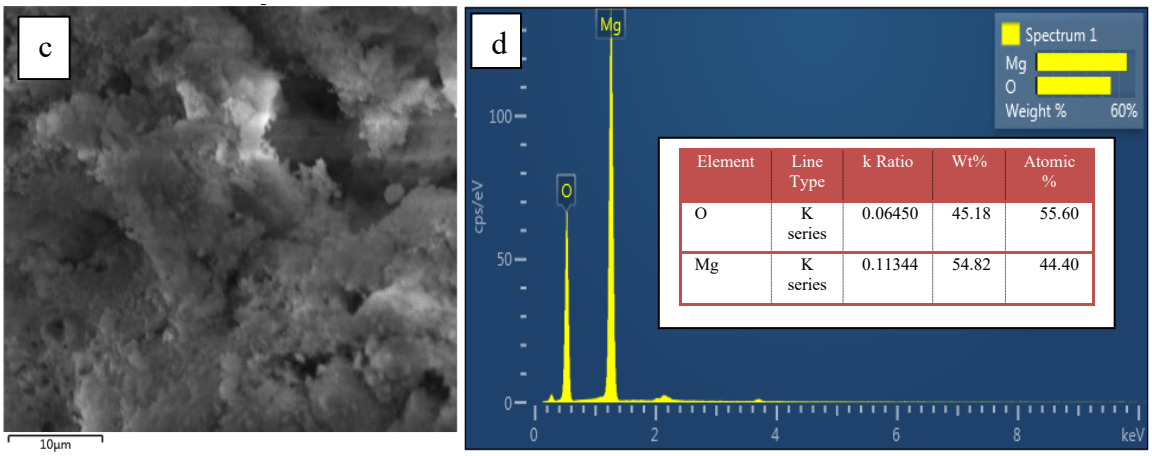

Figure 4: FE-SEM morphological images and EDX elemental characterization of MgO NPs synthesized using the ***P. granatum*** extract.

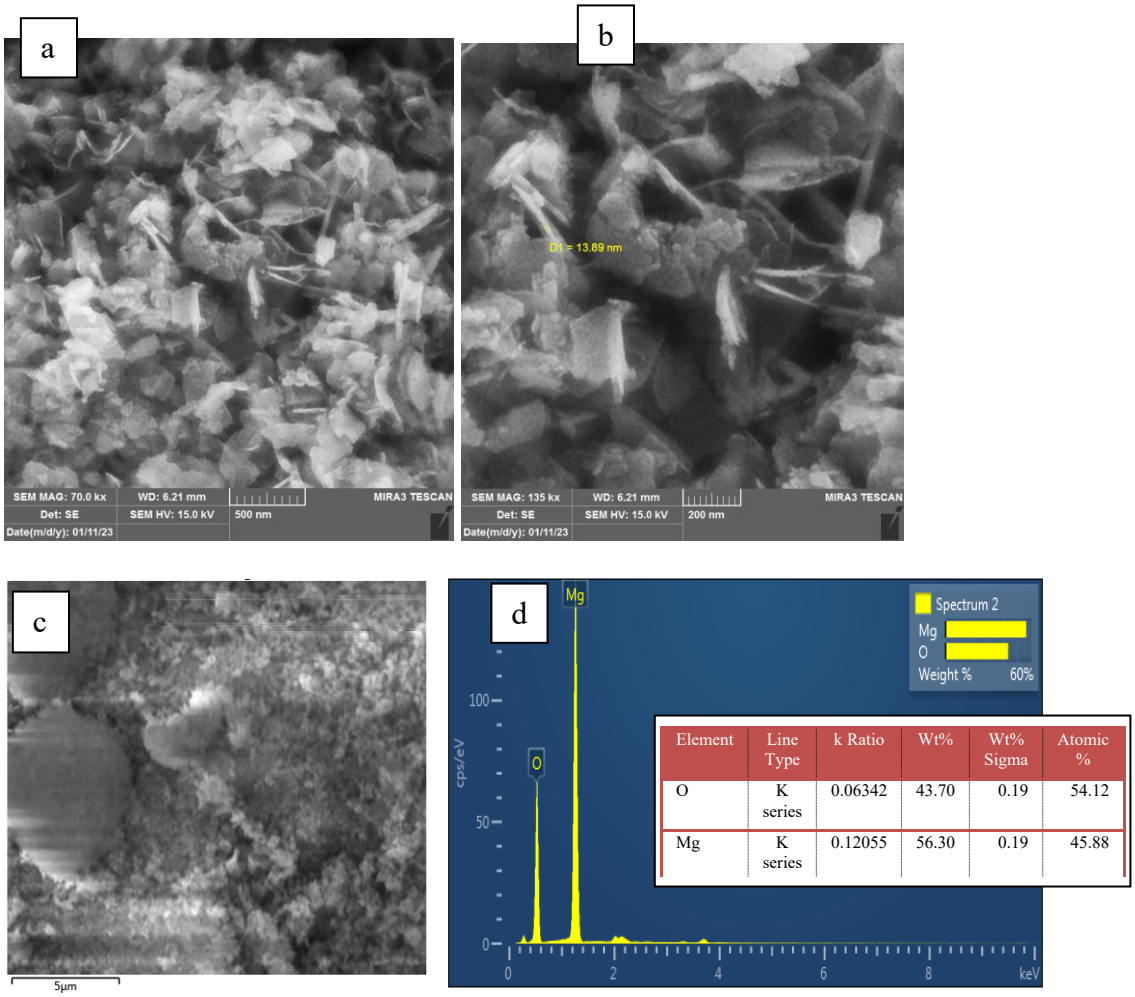

Figure 5: FE-SEM morphological images and EDX elemental characterization of MgO NPs synthesized using the *C. arabica* extract.

Technium Vol. 31, pp.9-45 (2026)
ISSN: 2668-778X
www.techniumscience.com

3.3 FTIR spectrum of MgO NPs using plant (*C. cyminum* , *P. granatum,* and *C. arabica*) extracts

The FTIR spectra of MgO NPs manufactured with three distinct plant-based extracts—*C. cyminum, P. granatum, and C. arabica*—are shown in Figure 6. The presence of hydroxyl groups, which could be the result of adsorbed water or polyphenolic chemicals in the plant extracts, is indicated by the broad absorption band seen at about 3468.99 cm^{-1}, which corresponds to the O–H stretching vibration. The C–H stretching vibrations of aliphatic compounds are responsible for the peaks seen at 2937 cm^{-1} and 2704 cm^{-1}, which indicate the presence of organic molecules left over after the bio-reductants. The stretching vibration of C=O groups, which may be caused by carboxylic acids, ketones, or ester functionalities, is linked to the absorption band at 1576.11 cm^{-1}. Furthermore, the presence of phenolic structures and alcohols from the plant-based stabilizing agents is indicated by the peaks at 1424.99 cm^{-1} and 1109.5 cm^{-1}, which are connected to C–C and C–O stretching vibrations. Most significantly, the distinctive bands seen at 414 to 646, 418 to 648, and 419 to 649 cm^{-1} attest to the creation of Mg–O bonds and indicate that MgO NPs were successfully synthesized using *C. cyminum, P. granatum, and C. arabica* extracts. These results show that plant extracts can be employed as both capping and reducing agents. They also show that the amount of organic residue varies depending on the extract utilized, which could affect the stability and surface characteristics of the MgO NPs, these results agree well with the reference [62].

A careful comparison was carried out, with an emphasis on the principal distinctive peaks corresponding to functional groups found in both samples. This comparison aimed to determine which functional groups in the plant extracts (*C. cyminum, P. granatum, and C. arabica)* were responsible for the MgO NPs stability and decrease. In both spectra, for example, peaks associated with hydroxyl (–OH), carbonyl (C=O), and phenolic groups were detected, suggesting that these biomolecules were involved in the creation of the MgO NPs. The greater quantity of hydroxyl-containing chemicals in *C. arabica* extract might explain the sharper O-H stretching vibrations found in the FTIR spectra of MgO nanoparticles generated using *C. arabica* extract compared to those made with *C. cyminum*. *C. arabica* extract grounds include phenolic chemicals, organic acids, and water-soluble hydroxyl groups, which can stay adsorbed on the surface of MgO NPs after production. Surface hydroxyl groups contribute to the noticeable O-H stretching bands at 3200-3600 cm^{-1}. In contrast, *C. cyminum* extract may include fewer hydroxyl-rich biomolecules or other chemical ingredients, resulting in lower O-H signals. This variation impacts surface chemistry, which can have an impact on nanoparticle stability, dispersibility, and catalytic or antibacterial activity [63].

Additionally, to comprehend the chemical interactions and bonding modifications taking place during MgO NPs production, shifts or variations in the strength and location of certain peaks between the plant extract and the MgO NPs spectra were examined. To support our study, it provided references to similar research that used a comparative approach [64-67].

Technium Vol. 31, pp.9-45 (2026)
ISSN: 2668-778X
www.techniumscience.com

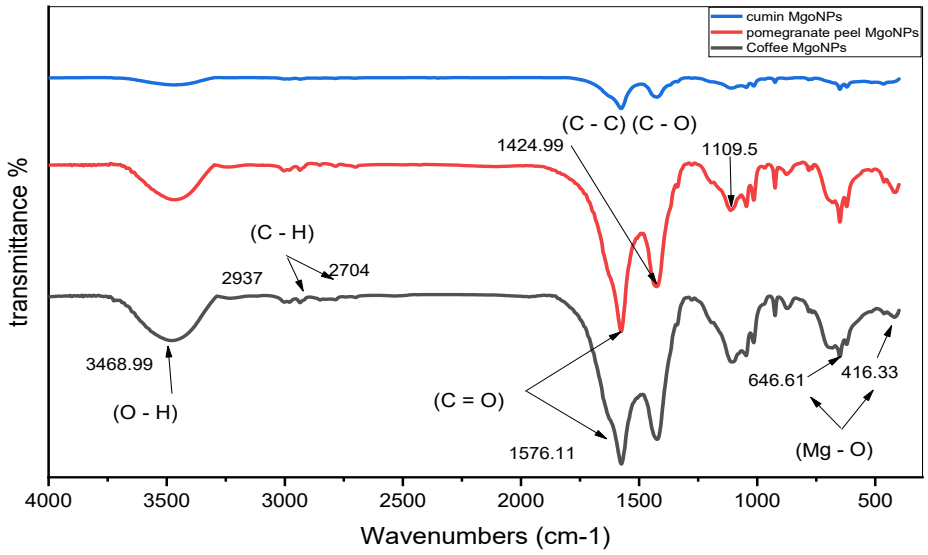

Figure 6: FTIR spectra of MgO NPs synthesized using *C. cyminum, P. granatum, and C. arabica* extracts.

3.4 Optical properties of MgO NPs using plant (*C. cyminum, P. granatum,* and *C. arabica*) extracts

The optical properties of MgO NPs synthesized using green synthesis methods were studied via UV-Vis absorption spectroscopy. Figure 7 shows the absorption spectra of MgO NPs prepared from *C. cyminum, P. granatum,* and *C. arabica* extracts. The absorption begins near the cutoff wavelength, marking the transition between absorption and transparency. The peak absorption wavelengths are observed at 194 nm (*C. cyminum*), 197 nm (*P. granatum*), and 200 nm (*C. arabica*). These results are consistent with previous studies. The low absorption values at these wavelengths are attributed to the quantum size effect, which modifies the electronic structure of the nanoparticles due to their high surface-to-volume ratio [68]. Figure 8 presents the Tauc plots which used to calculate the optical energy gaps [69]. The energy band gap of MgO NPs using the *C. cyminum, P. granatum,* and *C. arabica* extracts are 5.7 eV, 5.9 eV, and 5.8 eV, respectively.

These values are lower than the bulk value of 7.8 eV for MgO, confirming the impact of the quantum size effect. The reduced optical energy gaps reflect the changes in the electronic structure caused by the confinement of electrons and holes within the MgO NPs [70].

Technium Vol. 31, pp.9-45 (2026)
ISSN: 2668-778X
www.techniumscience.com

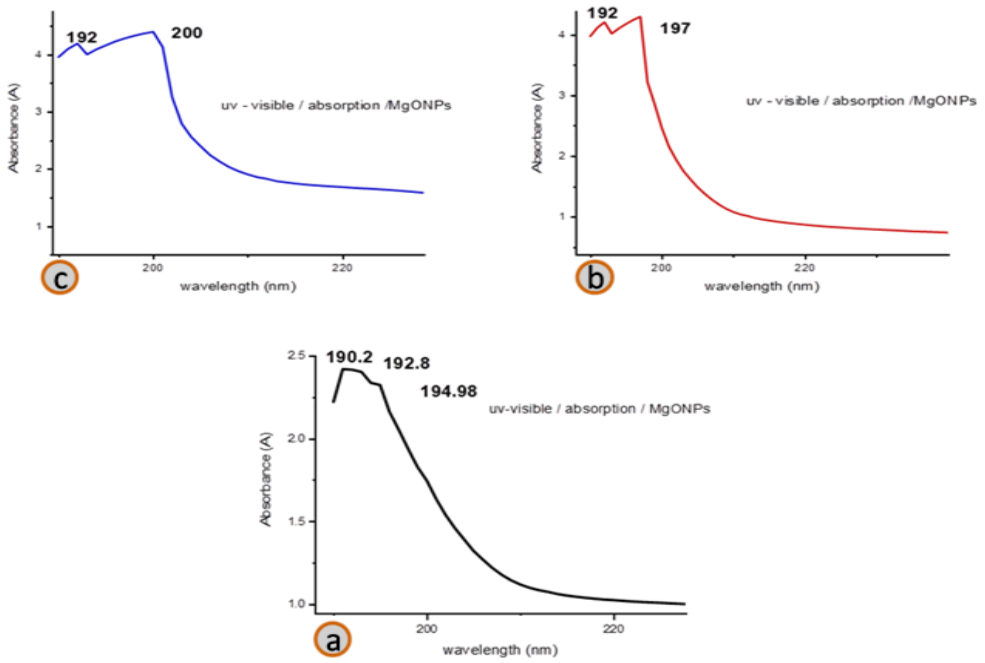

Figure 7: Absorption peak of MgO NPs synthesized from different plant extracts a) *C. cyminum*, b) *P. granatum*, and c) *C. arabica*.

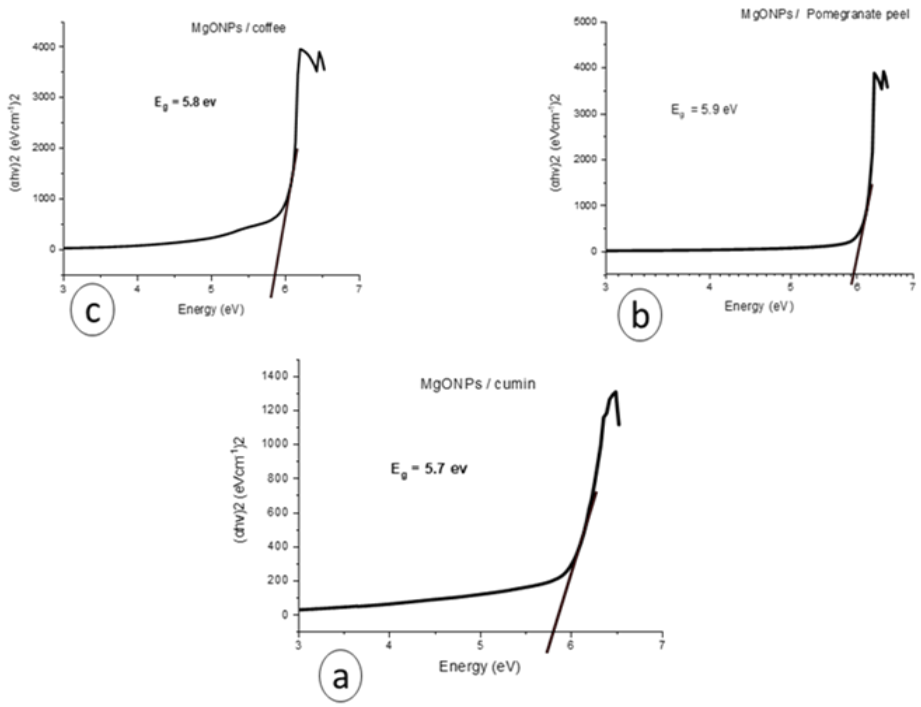

Figure 8: The energy band gap of MgO NPs synthesized from different plant extracts a) *C. cyminum* , b) *P. granatum,* and c) *C. arabica.*

3.5 Antibacterial Activity of MgO NPs using (*C. cyminum, P. granatum,* and *C. arabica*) plant extracts

This study examined the antibacterial activity of MgO NPs manufactured using various plant-based *C. cyminum, P. granatum, and C. arabica* extracts against two common bacterial strains: the Gram-positive Staphylococcus aureus ATTC25923 and the Gram-negative Escherichia coli ATTC25922. Müller-Hinton agar was used as the growth medium for the antibacterial tests, which were carried out using the time-kill assay and colony counting techniques. After being serially diluted to concentrations of 10^{-1}, 10^{-2}, 10^{-4}, and 10^{-5}, bacterial cultures at a concentration of 10^5 CFU/mL were incubated for 24 hours at 37 °C. Table 4 shows the antibacterial activity of MgO NPs using *C. cyminum, P. granatum, and C. arabica* extracts against gram-positive and gram-negative bacteria. According to the findings, MgO NPs have broad-spectrum antibacterial action and are significantly more efficient against Gram-positive S. aureus than Gram-negative E. coli. Electrostatic interactions between the positively charged Mg^{2+} ions and the bacterial cell membrane are responsible for this increased activity. These interactions cause NP attachment, membrane breakdown (pitting and cracking), and ultimately cell death [71].

Figure 9 (A-D) shows the antibacterial activity against Staphylococcus aureus using baseline control with concentrations (10^{-2}, 10^{-4}, 10^{-5}, and 10^{-6} CFU/mL. Figure 10, 11, and 12 shows the antibacterial activity against Staphylococcus aureus using *C. cyminum, P. granatum, and C. arabica* extracts with different concentrations (10^{-1}, 10^{-2}, 10^{-4}, and 10^{-5} CFU/mL. Figure 13 (A-D) shows the antibacterial activity against Escherichia coli using baseline control with concentrations (10^{-2}, 10^{-4}, 10^{-5}, and 10^{-6} CFU/mL. Figure 14, 15, and 16 shows the antibacterial activity against Escherichia coli using *C. cyminum, P. granatum, and C. arabica* extracts with concentrations (10^{-1}, 10^{-2}, 10^{-4}, and 10^{-5} CFU/mL.

With a 99.98% inhibition rate against S. aureus, MgO NPs synthesized from *C. cyminum* extract outperformed the other examined materials. *P. granatum* extract came in second with a 99.5% inhibition rate, and *C. arabica* extract came in third with a 68.39% inhibition rate. *C. arabica* (68.75%), *P. granatum* (71.87%), and *C. cyminum* (82.22%) had lower inhibition rates against E. coli. A thorough summary of the antibacterial activity and structural features of MgO NPs made from various plants emphasizing the relationship between NP morphology and biological activity.

The electrostatic interaction of MgO NPs with bacteria caused the bacterial wall damage and reduced antibacterial activity. MgO NPs are linked to the cell membrane via van der Waals and electrostatic interactions. After attaching to membrane proteins, MgO NPs impede bacterial activity, and a strong electrostatic interaction with spores causes cell death [72-74]. Furthermore, the defective nature of the surface and the positive charge of MgO NPs allow them to absorb halogen gases, resulting in significant interactions with negatively charged bacteria [75]. MgO NPs' antibacterial action can generate ROS-like $O_2\bullet-$, leading to lipid peroxidation in bacteria [76-77].

Increased surface area of MgO NPs leads to higher concentrations of $O_2^{\bullet-}$ in the environment, further destroying bacterial cell walls. When MgO NPs are fewer than 15 nm in size, the agglomeration effect becomes crucial due to the particles' extremely high surface energy. The enormous size of accumulated MgO NPs limits contact with microorganisms, lowering their antibacterial effects [78].

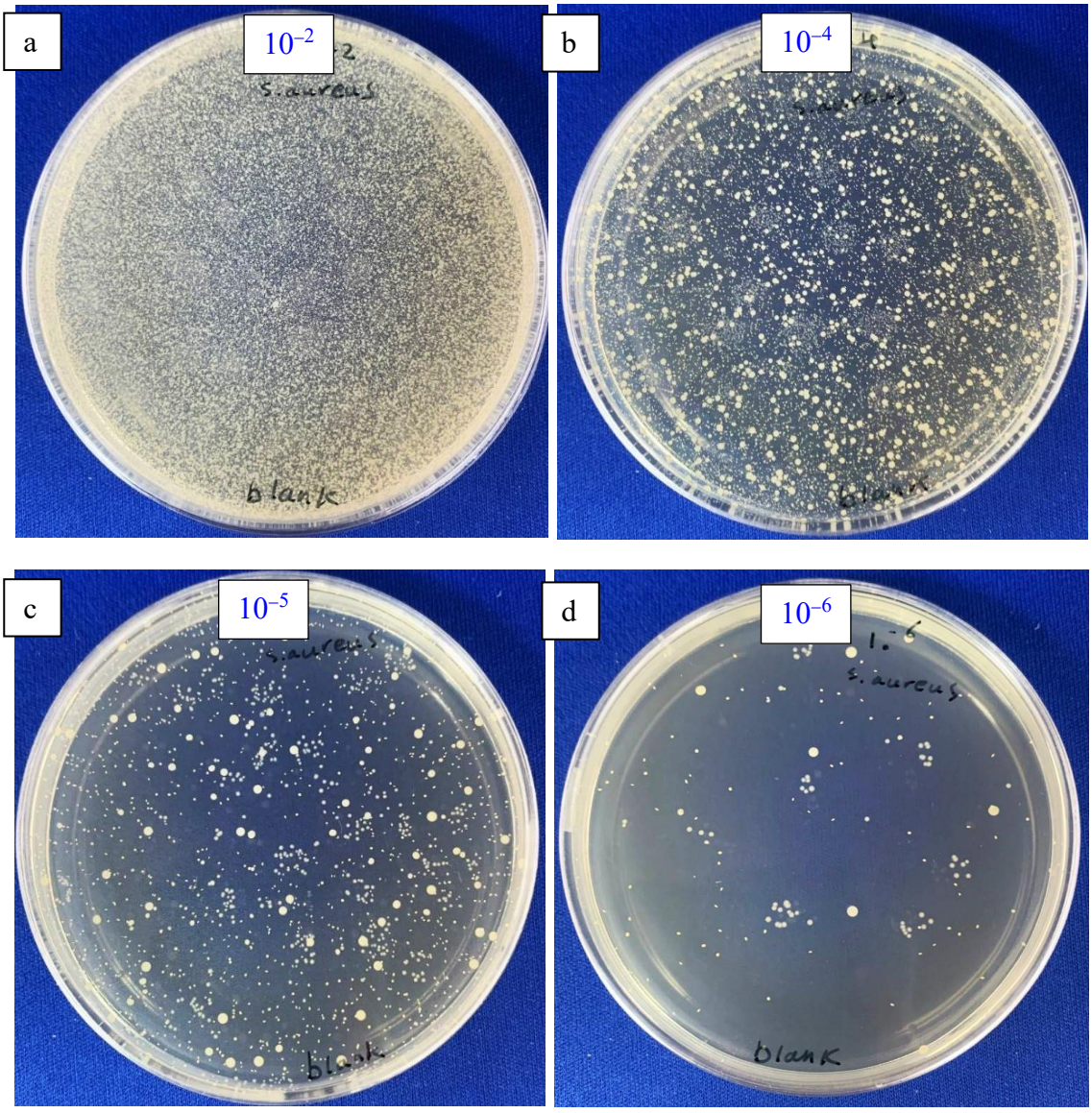

Figure 9: Antibacterial activity against Staphylococcus aureus using baseline control at varying concentrations, a) 10^{-2}, b) 10^{-4}, c) 10^{-5}, and d) 10^{-6}.

Technium Vol. 31, pp.9-45 (2026)
ISSN: 2668-778X
www.techniumscience.com

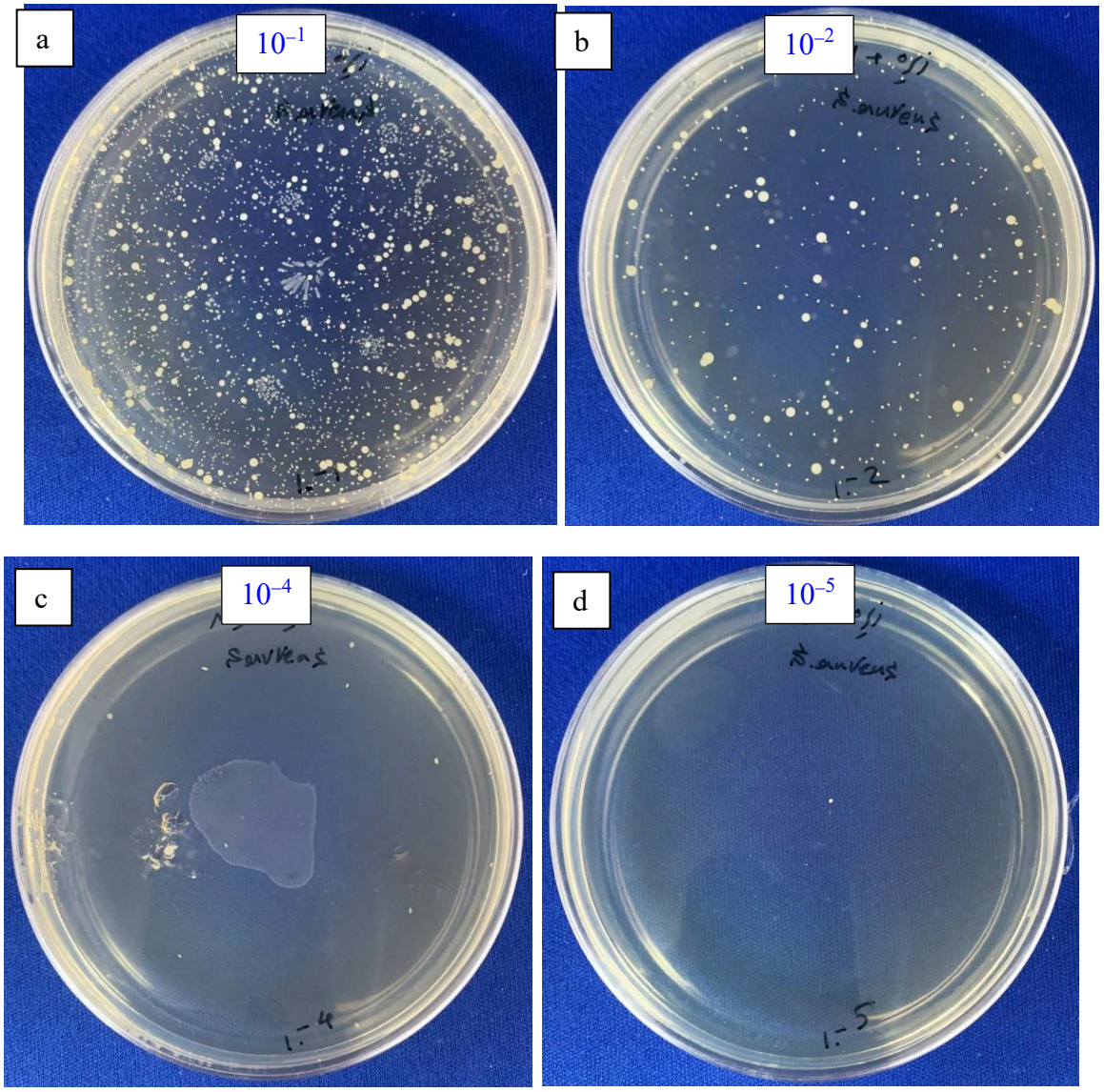

Figure 10: Antibacterial activity against Staphylococcus aureus using MgO NPs from C. *cyminum* extract at varying concentrations, a) 10^{-1}, b) 10^{-2}, c) 10^{-4}, and d) 10^{-5}.

Technium Vol. 31, pp.9-45 (2026)
ISSN: 2668-778X
www.techniumscience.com

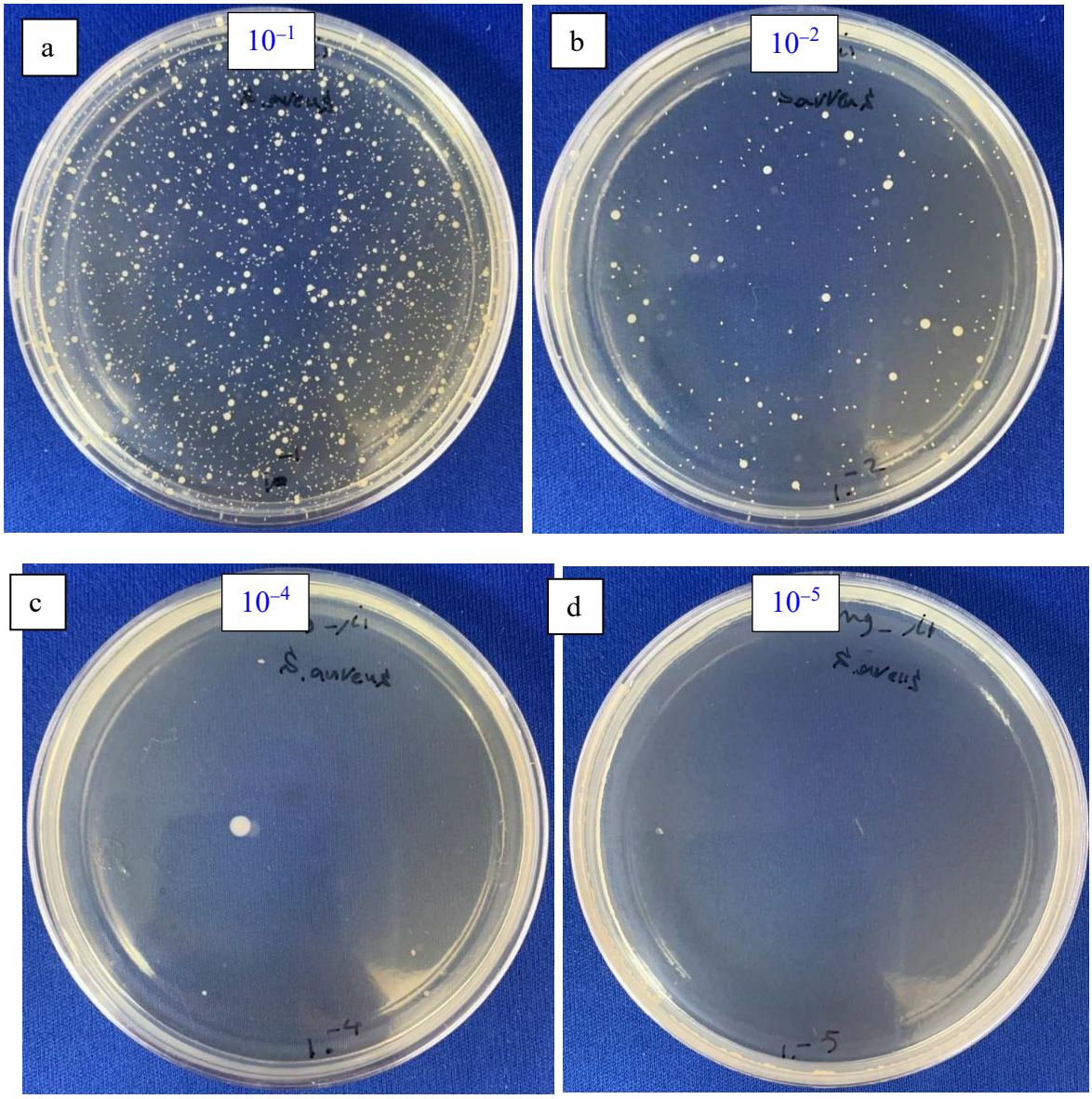

Figure 11: Antibacterial activity against Staphylococcus aureus using MgO NPs from *P. granatum* extract at varying concentrations, a) 10^{-1}, b) 10^{-2}, c) 10^{-4}, and d) 10^{-5}.

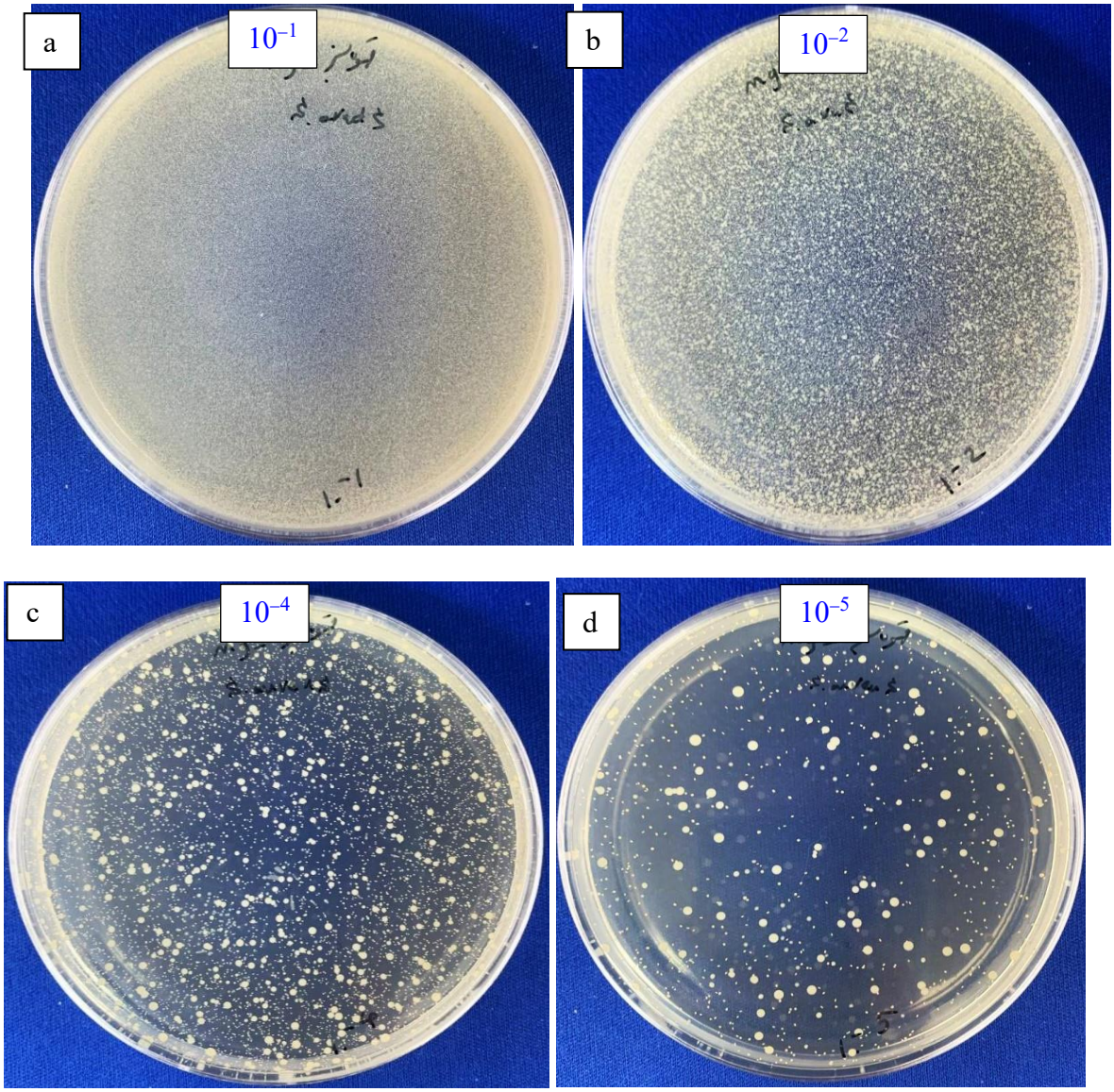

Figure 12: Antibacterial activity against Staphylococcus aureus using MgO NPs from *C. arabica* extract at varying concentrations, a) 10^{-1}, b) 10^{-2}, c) 10^{-4}, and d) 10^{-5}.

The control plates with serially diluted bacterial solutions demonstrating the baseline growth of S. aureus are shown in figure 9. The inhibitory zones for MgO NPs made from *C. cyminum, P. granatum,* and *C. arabica* extracts, respectively, at different concentrations are shown above. The studied NPs' dose-dependent antibacterial activity is demonstrated by the inhibition zones' growing size and clarity.

The control plates with serially diluted bacterial suspensions are shown in figure 13, which shows the E. coli growth baseline. The inhibitory zones for MgO NPs made from *C. cyminum, P. granatum,* and *C. arabica* extracts, respectively, at different concentrations are shown in figure 14, 15, and 16.The concentration-dependent antibacterial impact of the

nanoparticles is demonstrated by the size and clarity of the inhibition zones; *C. cyminum*-derived MgO NPs are the most effective against Gram-negative strain.

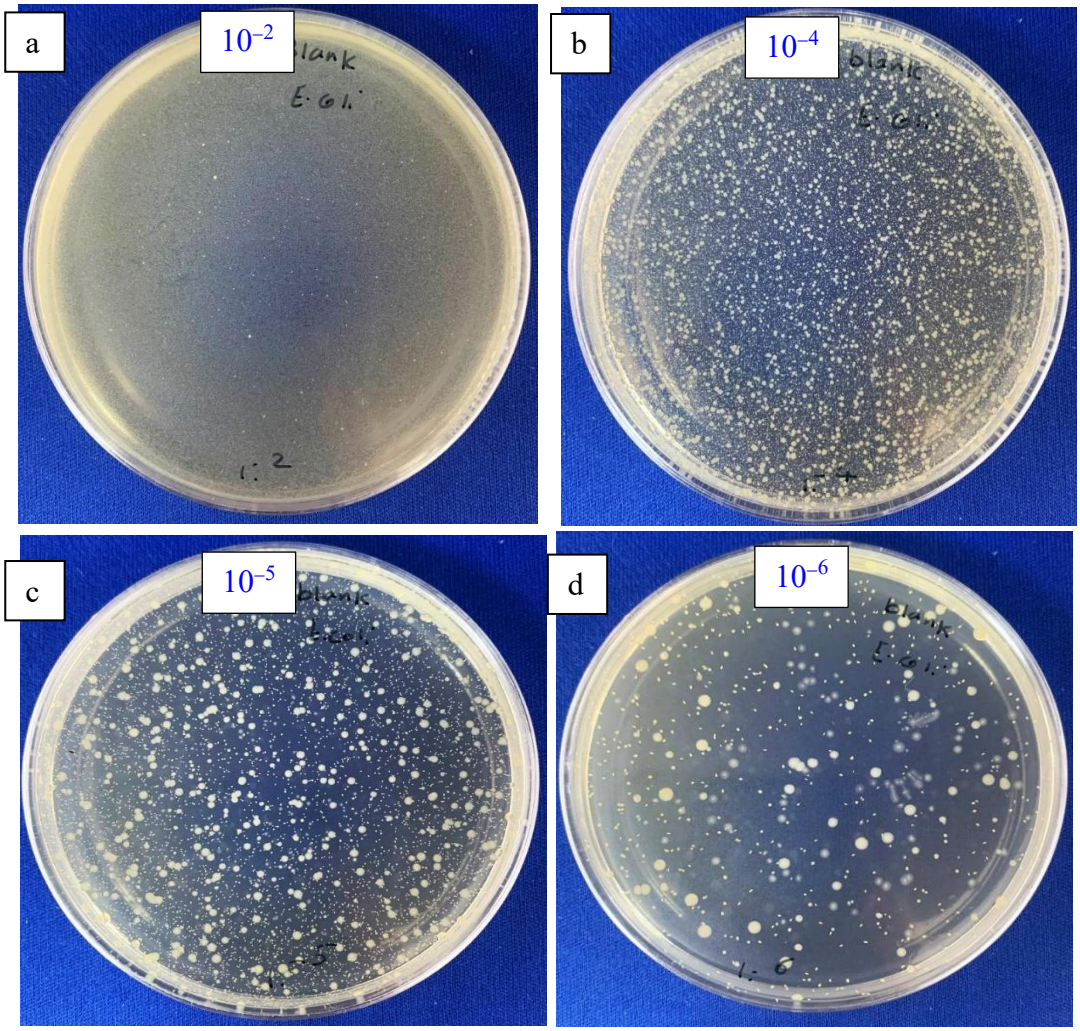

Figure 13: Baseline control for antibacterial activity against Escherichia coli at varying concentrations, a) 10^{-2}, b) 10^{-4}, c) 10^{-5}, and d) 10^{-6}.

Technium Vol. 31, pp.9-45 (2026)
ISSN: 2668-778X
www.techniumscience.com

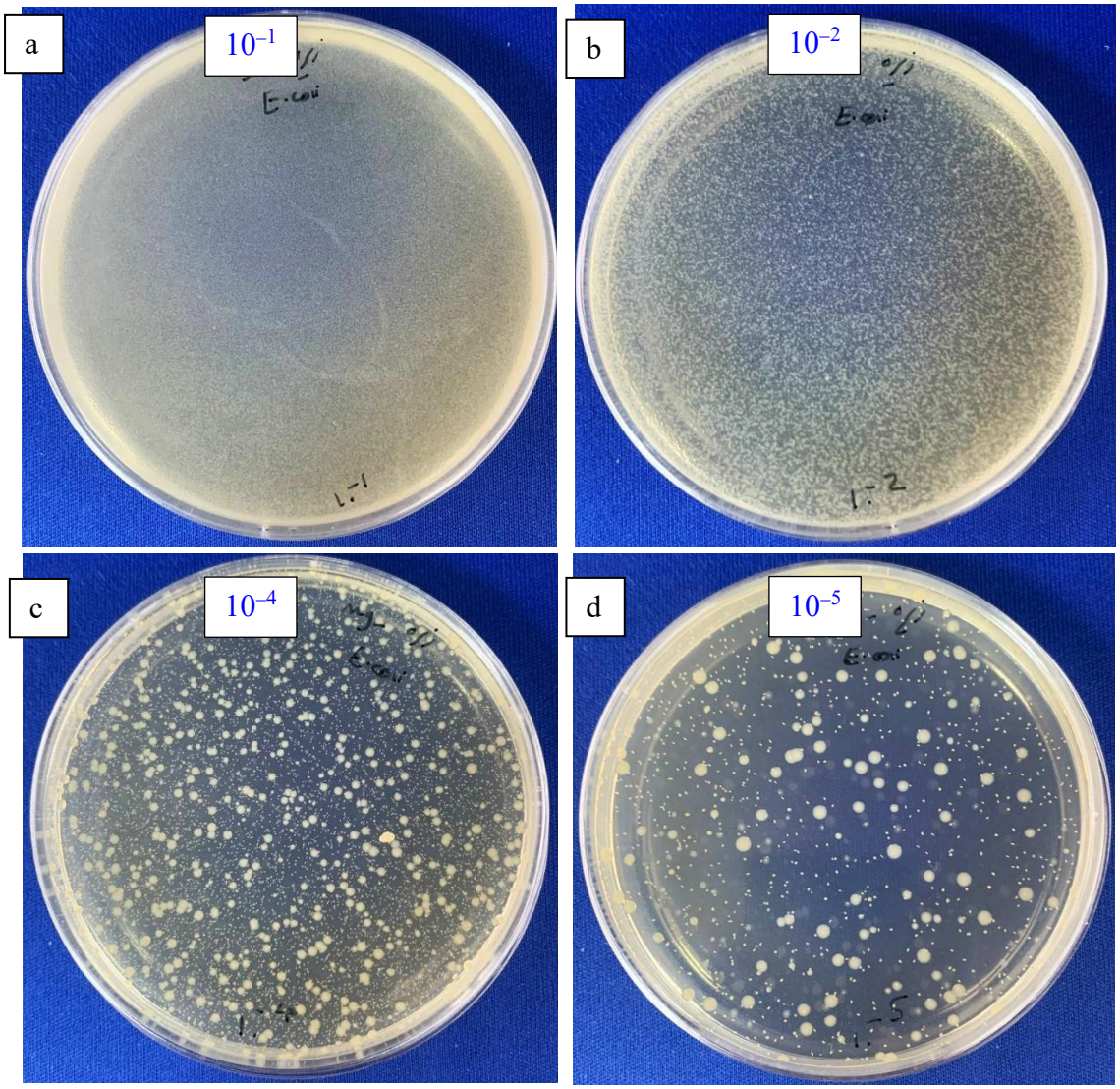

Figure 14: Antibacterial activity against Escherichia coli using MgO NPs from *C. cyminum* extract at varying concentrations, a) 10^{-1}, b) 10^{-2}, c) 10^{-4}, and d) 10^{-5}.

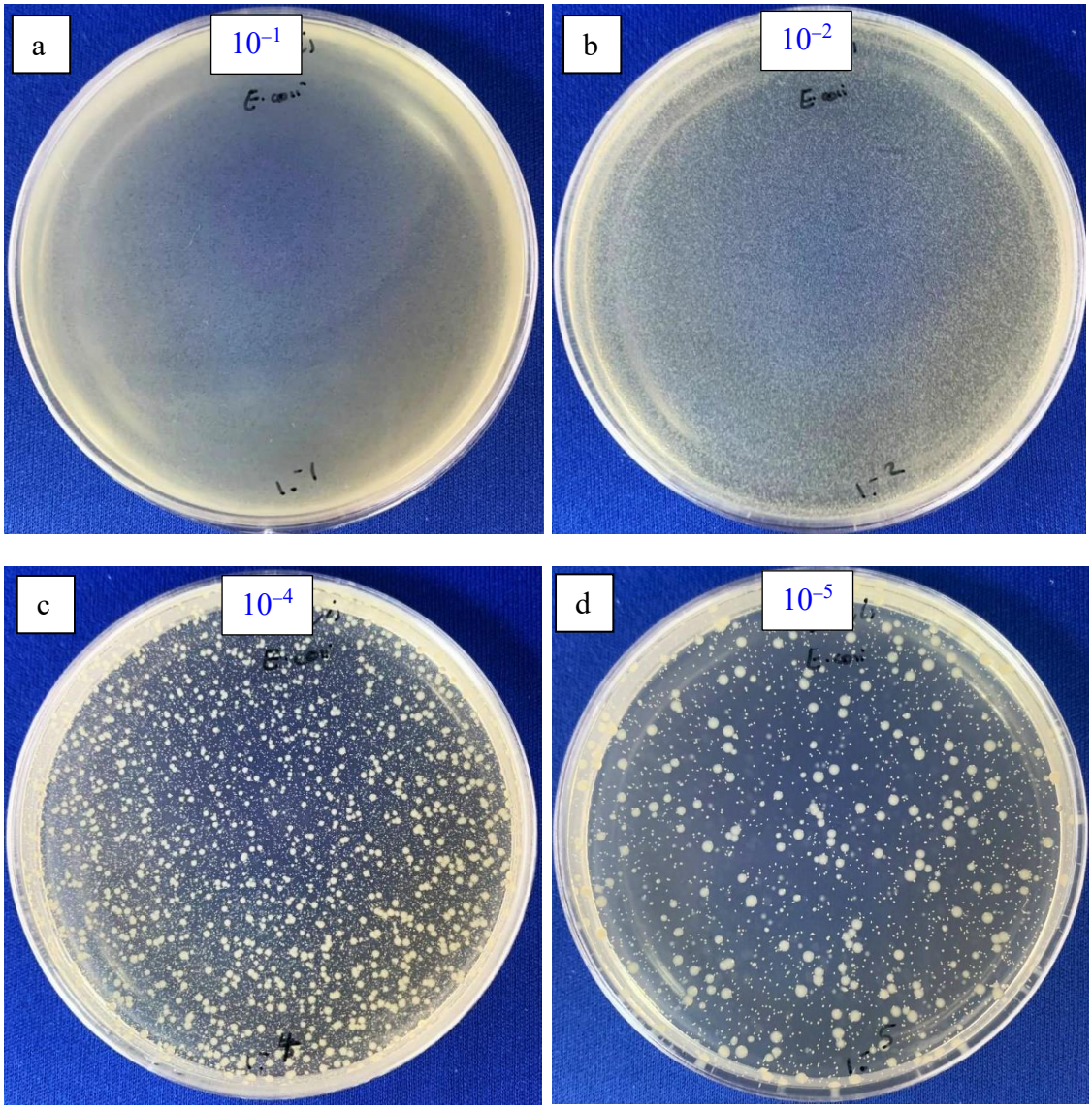

Figure 15: Antibacterial activity against Escherichia coli using MgO NPs from *P. granatum* extract at varying concentrations, a) 10^{-1}, b) 10^{-2}, c) 10^{-4}, and d) 10^{-5}.

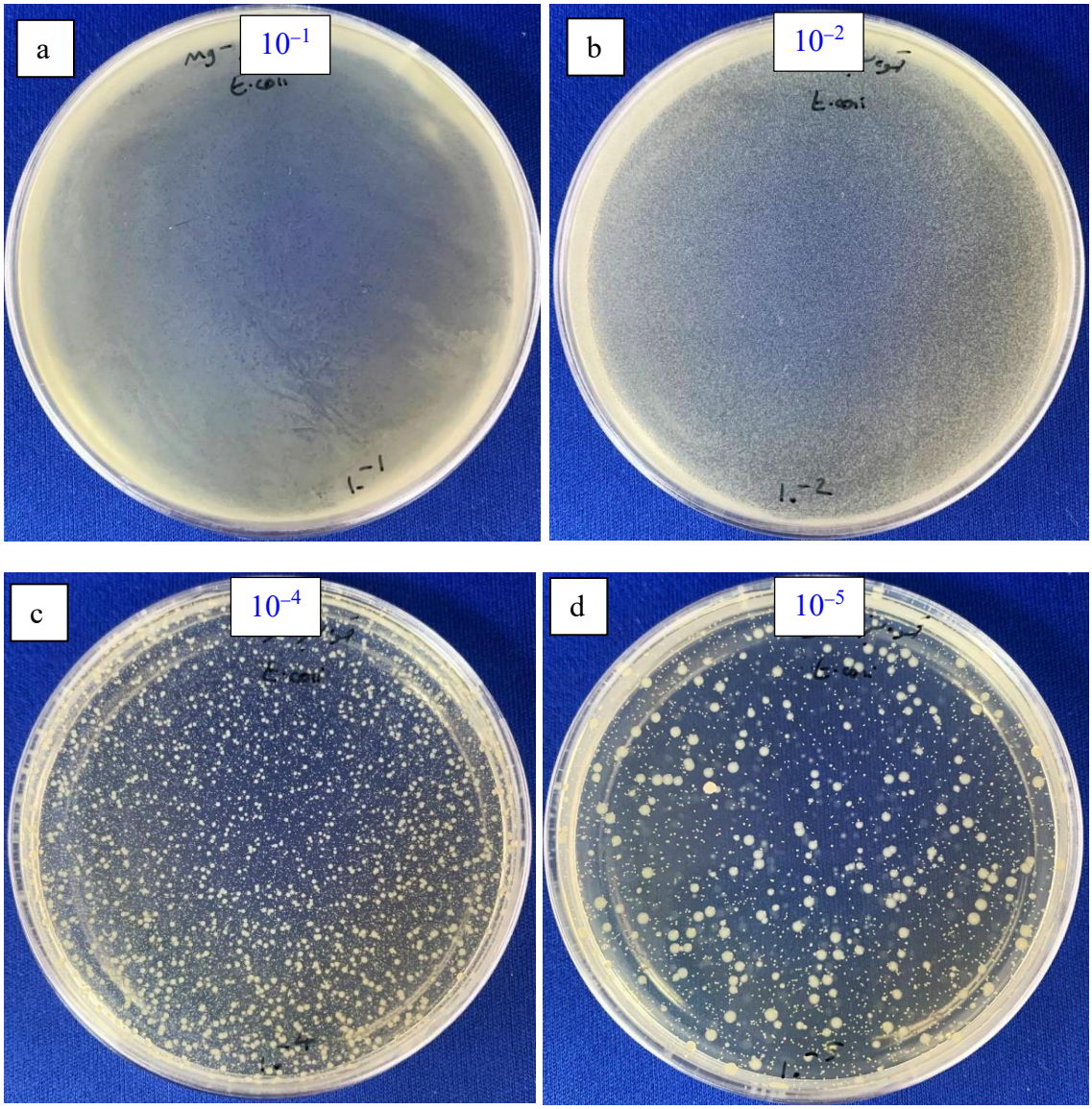

Figure 16: Antibacterial activity against Escherichia coli using MgO NPs from *C. arabica* extract at varying concentrations, a) 10^{-1}, b) 10^{-2}, c) 10^{-4}, and d) 10^{-5}.

A comparison of MgO NPs' antibacterial activity against specific gram-positive (Staphylococcus aureus) and gram-negative (Escherichia coli) bacterial strains utilizing extracts from *C. cyminum*, *P. granatum*, and *C. arabica* is shown in table 4.

Table 4: Comparative antibacterial efficacy of MgO NPs using *C. cyminum, P. granatum, and C. arabica* extracts against selected gram-positive (Staphylococcus aureus) and Gram-Negative (Escherichia coli) bacterial Strains.

Type of the bacteria	Type of Material	Number bacteria Inoculation in time (CFU/ml) (zero	Sample concentration	period of time Contact (the watch)	Results (CFU/ml)	inhibition ratio
Staphylococcus aureus ATCC25923	MgO NPs – *C. cyminum*	3.5×10^5	0.3 mg/ml	24	1.93×10^4	99.98 %
	MgO NPs - *P. granatum*		0.3 mg/ml		1.89×10^4	99.5%
	MgO NPs - *C. arabica*		0.3 mg/ml		5.12×10^7	68.39%
	Baseline *Control bacteria*		0.3mg/ml		1.62×10^8	-
Escherichia coli ATCC25922	MgO NPs – *C. cyminum*	1.72×10^5	0.3 mg/ml	24	5.69×10^7	82.22%
	MgO NPs - *P. granatum*		0.3 mg/ml		9.00×10^7	71.87%
	MgO NPs - *C. arabica*		0.3 mg/ml		1.00×10^8	68.75%
	Baseline *Control bacteria*		0.3 mg/ml		$3.2\times10_8$	-

3.6 Anticancer Activity of MgO NPs using (*C. cyminum*) extract

The current study's findings showed that MgO NPs synthesized using the *C. cyminum* extract significantly reduced the vitality of cancer cells, with cell viability percentages at 500 µg/ml and 1000 µg/ml being 56.63% and 44.42%, respectively. This suggests that cell viability is declining in a concentration-dependent manner. At the same concentrations, the cytotoxicity percentages were discovered to be 43.37% and 55.57%, respectively.

These results are depicted in Figures 17a and b, which clearly show that cell viability decreases as nanoparticle concentration rises. Due to MgO NPs' capacity to interact with cancer cells' plasma membranes and possibly trigger the production of reactive oxygen species (ROS), a lethal effect has been seen. Excessive ROS generation can cause oxidative stress, which can alter cellular processes, cause pathophysiological alterations, and ultimately lead to cell death [79]. Table 5 summarizes the anticancer activity of MgO NPs, highlighting their potential as promising agents for cancer therapy. The control sample (CO) showed 100% viability. Results

indicate a concentration-dependent increase in cytotoxicity. The IC_{50} value estimates that about 771.4 µg/mL of the tested chemical is required to block 50% of HeLa cell viability under the experimental circumstances after 24 hours of exposure. The control plates with serially diluted cancer solution demonstrating the CO growth are shown in Figures 17a and b. Table 6 revealed the present work results, which were compared with the previous studies.

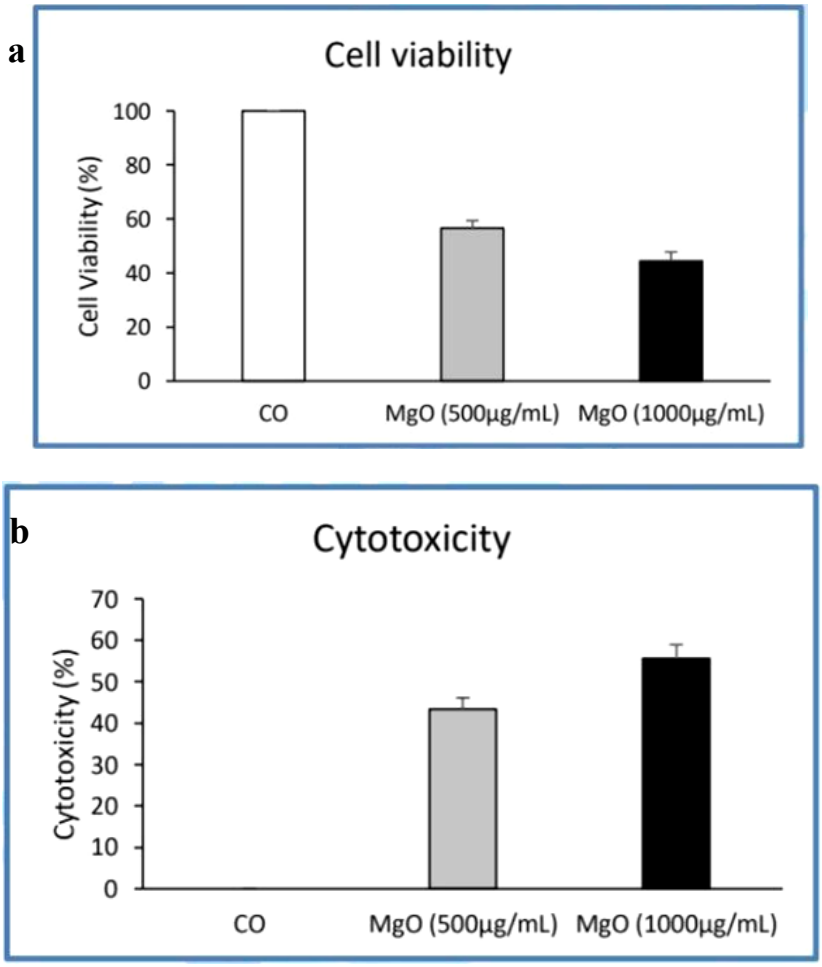

Figure 17: Cytotoxicity and cell viability of MgO NPs at different concentrations (a) Cell viability of cancer cells treated with MgO NPs at concentrations of 500 µg/mL and 1000 µg/mL, compared to the control (CO). (b) Corresponding cytotoxicity percentages for the same concentrations.

Table 5: Cytotoxic effect of MgO NPs on HeLa cells after 24 hours of exposure, showing cell viability and cytotoxicity percentages at concentrations of 500 µg/mL and 1000 µg/mL.

Material	Plant extract	Name of the cell line	Cell concentration (Number/ 200µl)	Call time the watch	Sample concentration (µg/ml)	Percent alive Mani cell	Percent toxicity cellular

MgO	***C. cyminum***	Hela cell	10000	24	500	56.63 %	43.37%
					1000	44.42 %	55.57%
					control sample (CO)	100	-

Table 6: The comparison of the present work results with academics previous studies.

Year	Authors	Plant extract	Material	Method	Reference
2022	Muslim A. Abid, et al.	Trigonella and Tomato	Iron oxide NPs	Simple chemical method	[81]
2023	Harjeet Singh , et al.	Plants	Nanomaterials	Green sythesis	[82]
2023	Duha A. Kadhim, et al.	Aloe Vera	Iron oxide NPs	Hydrothermal method	[83]
2024	Duha A. Kadhim, et al.	Marine shrimp shell	AgO/Fe2O3 NCs	Hydrothermal method	[84]
2025	Furkan Ulas, et al.	Plants	Ag NPs, ZnO NPs, NiO NPs, CuO NPs, Fe NPs	Green synthesis	[80]

4. Conclusion

C. cyminum, P. granatum, and *C. arabica* extracts were used to successfully create MgO NPs utilizing a green method. The final powders were very similar to MgO that is made commercially. This environmentally friendly method provides control over particle size and shape, which is in line with sustainable development goals. Because of the consistent heat treatment (500°C, 2 hours), all samples showed comparable optical characteristics and slight variations in crystal size. Notably, MgO NPs prepared using *C. cyminum* exhibited the strongest antibacterial and anticancer properties, with *P. granatum* coming in second. Differences in NPs size and shape are responsible for the increased bioactivity, underscoring the significance of nanostructure design in environmental and biomedical applications. Recent

results indicate MgO NPs manufactured from natural *plant* extracts have promising antibacterial and anticancer activity. As a first testing technique, the MTT test was used to assess the cytotoxic and cell viability effects. This study found that the inhibitory zones of gram-positive bacteria (S. aureus) were 99.98%, 99.50%, and 68.39%, respectively. Gram-negative bacteria (E. coli) had inhibition ratios of 82.22%, 71.87%, and 68.75%, in that order. Furthermore, MgO NPs made with extract from C. cyminum demonstrated 55.57% cell death against cervical cancer cells (HeLa line) at a dosage of 1000 µg/mL, suggesting substantial anticancer potential. To acquire an improved comprehension of the fundamental anticancer procedures, further studies such as cell cycle analysis utilizing flow cytometry and fluorescence microscopy using nuclear-specific dyes are proposed. Future research will focus on these sophisticated approaches to evaluate the cellular and molecular processes involved, as well as to support the future use of MgO NPs in biomedical applications.

CONFLICT OF INTEREST

The author declares that they have no conflict of interest.

Data Availability Statements

The data that support the finding of this study are available from the corresponding author upon reasonable request.

CRediT authorship contribution statement

Diyaa Y. Hussein: Funding acquisition, Formal analysis, Data curation.

Reference

[1] Malik, Shiza, Khalid Muhammad, and Yasir Waheed. "Nanotechnology: a revolution in modern industry." Molecules 28.2 (2023): 661.

[2] Singh, N. B., et al. "Nano revolution: exploring the frontiers of nanomaterials in science, technology, and society." Nano-Structures & Nano-Objects 39 (2024): 101299.

[3] Palit, Sukanchan, and Chaudhery Mustansar Hussain. "Recent advances in green nanotechnology and the vision for the future." Green Metal Nanoparticles: Synthesis, Characterization and their Applications (2018): 1-21.

[4] Litter, Marta I., and Arslan Ahmad. "The world of nanotechnology." Industrial applications of nanoparticles. CRC Press, 2023. 1-15.

[5] Nasrollahzadeh, Mahmoud, et al. "An introduction to nanotechnology." Interface science and technology. Vol. 28. Elsevier, 2019. 1-27.

[6] Hassan, Saad El-Din, et al. "Rhizopus Oryzae-mediated green synthesis of magnesium oxide nanoparticles (MgO-NPs): A promising tool for antimicrobial, mosquitocidal action, and tanning effluent treatment." Journal of Fungi 7.5 (2021): 372.

[6] Saied, Ebrahim, et al. "The catalytic activity of biosynthesized magnesium oxide nanoparticles (MgO-NPs) for inhibiting the growth of pathogenic microbes, tanning effluent treatment, and chromium ion removal." Catalysts 11.7 (2021): 821.

[7] Khan, Mohammad Rashid, et al. "Evaluation of biogenically synthesized MgO NPs anticancer activity against breast cancer cells." Saudi Journal of Biological Sciences 31.1 (2024): 103874.

[8] Prakash kumar, M.R. Ramesh, Mrityunjay Doddamani, Joghee Suresh, Ragunath Lingaraj, Green synthesis of CuO/MgO/ZnO nanoparticles using Costus pictus leaf extract for effective antibacterial applications, Materials Letters, Volume 359, 2024, 135918, ISSN 0167-577X.

[9] Priyadarshini, Barsharani, et al. "Effect of Zn doping on dielectric properties of MgO nanoparticles synthesized by microwave-assisted combustion route." Materials Letters 304 (2021): 130645.

[10] Ahmed, Temoor, et al. "Antibacterial potential of green magnesium oxide nanoparticles against rice pathogen Acidovorax oryzae." Materials Letters 282 (2021): 128839.

[11] Balakrishnan, G., et al. "Microstructure, optical and photocatalytic properties of MgO nanoparticles." Results in Physics 16 (2020): 103013.

[12] Zwijnenburg, Martijn A. "The effect of particle size on the optical and electronic properties of magnesium oxide nanoparticles." Physical Chemistry Chemical Physics 23.38 (2021): 21579-21590.

[13] Essien, Enobong R., et al. "Biogenic synthesis of magnesium oxide nanoparticles using Manihot esculenta (Crantz) leaf extract." International Nano Letters 10.1 (2020): 43-48.

[14] Fadhil, Fattin A., et al. "Optical properties of MgO NPs produced by laser ablation in liquid." AIP Conference Proceedings. Vol. 2372. No. 1. AIP Publishing, 2021.

[15] Ijaz, Irfan, et al. "Detail review on chemical, physical and green synthesis, classification, characterizations and applications of nanoparticles." Green chemistry letters and reviews 13.3 (2020): 223-245.

[16] Kirubakaran, Dharmalingam, et al. "A comprehensive review on the green synthesis of nanoparticles: advancements in biomedical and environmental applications." Biomedical Materials & Devices (2025): 1-26.

[17] Ying, Shuaixuan, et al. "Green synthesis of nanoparticles: Current developments and limitations." Environmental Technology & Innovation 26 (2022): 102336.

[18] Jain, Kavya, et al. "Rethinking nanoparticle synthesis: a sustainable approach vs. traditional methods." Chemistry–An Asian Journal 19.21 (2024): e202400701.

[19] lsaiari, Norah Salem, et al. "Plant and microbial approaches as green methods for the synthesis of nanomaterials: synthesis, applications, and future perspectives." Molecules 28.1 (2023): 463.

[20] Khan, Fahad, et al. "Prospects of algae-based green synthesis of nanoparticles for environmental applications." Chemosphere 293 (2022): 133571.

[21] Adeyemi, Jerry O., et al. "Plant extracts mediated metal-based nanoparticles: synthesis and biological applications." Biomolecules 12.5 (2022): 627.

[22] Villagrán, Zuamí, et al. "Plant-based extracts as reducing, capping, and stabilizing agents for the green synthesis of inorganic nanoparticles." Resources 13.6 (2024): 70.

[23] Hudlikar, Manish, et al. "Green synthesis of TiO2 nanoparticles by using aqueous extract of Jatropha curcas L. latex." Materials Letters 75 (2012): 196-199.

[24] Rani, Anita, and Manoj Kumar, eds. Plant Mediated Synthesis of Metal Nanoparticles. Bentham Science Publishers, 2024.

[25] Begum, Shabaaz JP, et al. "Recent advances in green synthesis, characterization, and applications of bioactive metallic nanoparticles." Pharmaceuticals 15.4 (2022): 455.

[26] Fouda, Amr, et al. "The antimicrobial and mosquitocidal activity of green magnesium oxide nanoparticles synthesized by an aqueous peel extract of Punica granatum." Chemistry 5.3 (2023): 2009-2024.

[27] Ilavenil, K. K., V. Senthilkumar, and A. Kasthuri. "Green synthesis of metal nanoparticles from three medicinal plants: a review of environmental and health applications." Discover Catalysis 2.1 (2025): 3.

[28] Aygun, Aysenur, et al. "Biogenic platinum nanoparticles using black cumin seed and their potential usage as antimicrobial and anticancer agent." Journal of pharmaceutical and biomedical analysis 179 (2020): 112961.

[29] Abbas, Murtadha Kudair, and M. Sh Hashim. "Production of bioactive MgO nanoparticles via anodic technique." Journal of Physics: Conference Series. Vol. 2322. No. 1. IOP Publishing, 2022.

[30] Dinparvar, S., Bagirova, M., Allahverdiyev, A. M., Abamor, E. S., Safarov, T., Aydogdu, M., & Aktas, D. (2020). A nanotechnology-based new approach in the treatment of breast

cancer: Biosynthesized silver nanoparticles using Cuminum cyminum L. seed extract. *Journal of Photochemistry and Photobiology B: Biology*, *208*, 111902.

[31] V. Jayavarsha, S. Rajeshkumar, T. Lakshmi, G. Sulochana Green synthesis of selenium nanoparticles study using clove and cumin and its anti-inflammatory activity J. Complement Med. Res., 13 (2022), p. 84.
[32]F. Adibian, R.S. Ghaderi, Z. Sabouri, J. Davoodi, M. Kazemi, K. Ghazvini, M. Youssefi, S. Soleimanpour, M. Darroudi Green synthesis of selenium nanoparticles using Rosmarinus officinalis and investigated their antimicrobial activity BioMetals (2022), pp. 1-12.
[33] N. Siddiqui, K. Pal, P. Karmakar, M.M. Islam, S. Mukhopadhyay A dual role of cumin-seed extract towards the silver nanoparticle synthesis and stabilisation and its potential for antibacterial and anticancer activities through oxidative damage Adv. Nat. Sci.: Nanosci. Nanotechnol., 11 (2020), Article 025019.

[34] Farouk, S. M., Abu-Hussien, S. H., Abd-Elhalim, B. T., Mohamed, R. M., Arabe, N. M., Hussain, A. A., ... & Galal, A. (2023). Biosynthesis and characterization of silver nanoparticles from Punica granatum (pomegranate) peel waste and its application to inhibit foodborne pathogens. *Scientific Reports*, *13*(1), 19469.

[35] Kavin, T., Murugaiyah, V., Tan, J. K., Kassim, M. N. I., Ramakrishna, S., & Vigneswari, S. (2025). Eco-friendly synthesis of silver nanoparticles using Coffea arabica husk for enhanced antibacterial and anti-cancer applications. *Biomass and Bioenergy*, *194*, 107625.

[36] Deepika, S., Selvaraj, C. I., & Roopan, S. M. (2020). Screening bioactivities of Caesalpinia pulcherrima L. swartz and cytotoxicity of extract synthesized silver nanoparticles on HCT116 cell line. *Materials Science and Engineering: C*, *106*, 110279.

[37] Deepika, S., Selvaraj, C. I., & Anbalagan, M. (2018). Phytochemical characterization and cancer cell line cytotoxicity of Clitoria ternatea. ||| *Bangladesh Journal of Pharmacology*|||, *13*(4), 349-352.

[38] Hadkar, V. M., Mohanty, C., & Selvaraj, C. I. (2024). Biopolymeric nanocarriers in cancer therapy: unleashing the potency of bioactive anticancer compounds for enhancing drug delivery. *RSC advances*, *14*(35), 25149-25173.

[39] Jang, S. J., Yang, I. J., Tettey, C. O., Kim, K. M., & Shin, H. M. (2016). In-vitro anticancer activity of green synthesized silver nanoparticles on MCF-7 human breast cancer cells. *Materials Science and Engineering: C*, *68*, 430-435.

[40] Kummara, S., Patil, M. B., & Uriah, T. (2016). Synthesis, characterization, biocompatible and anticancer activity of green and chemically synthesized silver nanoparticles–a comparative study. *Biomedicine & Pharmacotherapy*, *84*, 10-21.

[41] Kadhim, D. A., Abid, M. A., Abdulghany, Z. S., Yahya Alhatem, J., Kadhim, S. A., Aziz, W. J., & Al-Marjani, M. F. (2022). Iron oxide nanoparticles synthesized using plant (Beta vulgaris and Punica granatum) extracts for a breast cancer cell line (MCF-7) cytotoxic assay. *Materials Technology*, *37*(13), 2436-2444.

[42] Abid, M. A., & Kadhim, D. A. (2022). Synthesis of iron oxide nanoparticles by mixing chilli with rust iron extract to examine antibacterial activity. *Materials Technology*, *37*(10), 1494-1503.

[43] Kadhim, D. A., Abid, M. A., & Salih, W. M. (2024). Photocatalytic activity for degradation of methylene blue dye-mediated nanocomposite-copper oxide/graphene oxide preparation from blood solution via hydrothermal method with laser irradiation. *Vacuum*, *228*, 113481.

[44] Ali, S. Q., Kadhim, D. A., Mohammed, A. H., Mohammed, R. S., Abid, M. A., & Athari, S. A. (2025). Green synthesis of α-MnO2/Ag nanocomposite using Malva parviflora (Khabbaz) extract for antimicrobial activity. *Nano-Structures & Nano-Objects*, *42*, 101467.

[45] Sishu, N. K., Karunakaran, M. K. R., Hadkar, V. M., Mohanty, C., Sharmila, A., Selvaraj, C. I., & Babu, N. G. (2025). Phyto-mediated synthesis of SnO 2 nanoparticles using Croton malabaricus Bedd. for its antioxidant, antibacterial, hemocompatibility properties and photocatalytic activity. *New Journal of Chemistry*, *49*(2), 536-552.

[46] Sishu, N. K., & Selvaraj, C. I. (2025). Bio-fabrication of Cichorium intybus L. root aqueous extract mediated ZnO nanoparticle (CIRAE-ZnO NP) for its promising therapeutic applications. *Green Chemistry Letters and Reviews*, *18*(1), 2489461.

[47] Sharmila, A., & Selvaraj, C. I. (2025). Sustainable synthesis of Au-ZnO nanocomposites for effective photocatalytic degradation of methylene blue in wastewater and therapeutic applications. *Ceramics International*.

[48] Sishu, N. K., & Selvaraj, C. I. (2025). Phytochemical Profiling, Bioactive Potential and In Silico Analysis of Kydia calycina Roxb. Leaf Extracts. *Chemistry & Biodiversity*, e202403132.

[49] Osman, A. I., Zhang, Y., Farghali, M., Rashwan, A. K., Eltaweil, A. S., Abd El-Monaem, E. M., ... & Yap, P. S. (2024). Synthesis of green nanoparticles for energy, biomedical, environmental, agricultural, and food applications: A review. Environmental Chemistry Letters, 22(2), 841-887.

[50] Al-Hatem, J. Y., Kadhim, D. A., & Abid, M. A. (2025). Developing A Nano-Fertilizer of Iron Oxide NPs Using Yeast Extract and Studying its Effectiveness on the Growth and Germination of Nigella sativa Seeds. *Basrah Journal of Agricultural Sciences*, *38*(1), 235-247.

[51] Kadhim, D. A., Abid, M. A., Latif, L. A., Salih, W. M., & Al-Kazazz, F. F. (2024). Blood-liquid extract inhibits bacteria through diffusion-mediated nano-CuO. *Nano-Structures & Nano-Objects*, *37*, 101105.

[52] Kadhim, D. A., Abid, M. A., & Salih, W. M. (2024). Development of iron oxide nanoparticles using egg peel (brown) extract as a useful tool for removing the MB dye. *Materials Science and Engineering: B*, *300*, 117104.

[53] Kadhim, F. J., Bedoui, M. H., Kadhim, D. A., & Abid, M. A. (2025). Novel comparison of silver oxide nanoparticle preparation from mixing the wild shrimp extract with Ag2NO3 salt via hydrothermal with and without laser for staphylococcus bacteria activity. *Optics & Laser Technology*, *182*, 112109.

[54] Arshad, F.; Naikoo, G.A.; Hassan, I.U.; Chava, S.R.; El-Tanani, M.; Aljabali, A.A.; Tambuwala, M.M. Bioinspired and Green Synthesis of Silver Nanoparticles for Medical Applications: A Green Perspective. *Appl. Biochem. Biotechnol.* **2024**, *196*, 3636–3669.

[55] Asadi, Sura M. Al, et al. "The effect of MgO nanoparticles on structure and optical properties of PVA-PAAm blend." Research Journal of Pharmacy and Technology 12.6 (2019): 2768-2771.

[56] Mahdi, M. M., Ali, A. M., Alalousi, M. A., Kadhim, D. A., & Abid, M. A. (2024). Developing a copper-zinc-aluminum alloying technique by vacuum thermal deposition after irradiation by gamma rays (NaI (Ti)) with stabilized zinc metal. *Vacuum*, *219*, 112676.

[57] Abbas, I. K., & Adim, K. A. (2023). Synthesis and characterization of magnesium oxide nanoparticles by atmospheric non-thermal plasma jet. *Kuwait Journal of Science*, *50*(3), 223-230.

[58] Kireev P., Semiconductors Physics, Translated from Russian by M. Samokhvalove, *MIR Puplishers*, Moscow (1978).

[59] Barzegar, M., Ahmadvand, D., Sabouri, Z., & Darroudi, M. (2024). Phytoextract-mediated synthesis of magnesium oxide nanoparticles using Caccinia macranthera extract and examination of their photocatalytic and anticancer effects. *Materials Research Bulletin*, *169*, 112514.

[60] AlHoly, T., & Khaddam, W. (2023). Extracellular Synthesis of Magnesium Oxide at Nano and Bulk Scale: Antifungal Effect Against Candida albicans, Aspergillus niger. *Jordan Journal of Pharmaceutical Sciences*, *16*(4).

[61] Sambandam, T., Karuppasamy, G., Perumal, G., & Rajasingh, E. C. (2025). Liquid phase preparation and characterization of MgO nanoparticles and their butchery activities against dental bacterial pathogens and human cervical cancer cell line. *Journal of Photochemistry and Photobiology B: Biology*, *262*, 113084.

[62] Harishkumar, R., & Selvaraj, C. I. (2020). Lotusine, an alkaloid from Nelumbo nucifera (Gaertn.), attenuates doxorubicin-induced toxicity in embryonically derived H9c2 cells. *In Vitro Cellular & Developmental Biology-Animal*, *56*(5), 367-377.

[63] Dinesh, M., Roopan, S. M., Selvaraj, C. I., & Arunachalam, P. (2017). Phyllanthus emblica seed extract mediated synthesis of PdNPs against antibacterial, heamolytic and cytotoxic studies. *Journal of Photochemistry and Photobiology B: Biology*, *167*, 64-71.

[64] Deepika, S., Selvaraj, C. I., & Anbalagan, M. (2018). Phytochemical characterization and cancer cell line cytotoxicity of Clitoria ternatea. ||| *Bangladesh Journal of Pharmacology*|||, *13*(4), 349-352.

[65] Deepika, S., Selvaraj, C. I., & Roopan, S. M. (2020). Screening bioactivities of Caesalpinia pulcherrima L. swartz and cytotoxicity of extract synthesized silver nanoparticles on HCT116 cell line. *Materials Science and Engineering: C*, *106*, 110279.

[66] Sharmila, A., & Selvaraj, C. I. (2024). LC–MS/MS-QTOF analysis of Anodendron parviflorum (Roxb.) leaves extract and exploring its antioxidant, antimicrobial, and cytotoxic potential. *Future Journal of Pharmaceutical Sciences*, *10*(1), 122.

[67] Dinesh, M., Deepika, S., HarishKumar, R., Selvaraj, C. I., & Roopan, S. M. (2018). Evaluation of octyl-β-D-glucopyranoside (OGP) for cytotoxic, hemolytic, thrombolytic, and antibacterial activity. *Applied biochemistry and biotechnology*, *185*(2), 450-463.

[68] Sim, H. T., Gençaslan, M., & Merdan, M. (2024). Synthesis of MgO nanoparticles via the sol-gel method for antibacterial applications, investigation of optical properties and comparison with commercial MgO. *Discover Applied Sciences*, *6*(11), 577.

[69] Haryński, Ł., Olejnik, A., Grochowska, K., & Siuzdak, K. (2022). A facile method for Tauc exponent and corresponding electronic transitions determination in semiconductors directly from UV–Vis spectroscopy data. *Optical Materials*, *127*, 112205.

[70] Varshney, D., & Dwivedi, S. (2015). On the synthesis, structural, optical and magnetic properties of nano-size Zn–MgO. *Superlattices and Microstructures*, *85*, 886-893.

[71] Rodríguez-Hernández, A. P., Vega-Jiménez, A. L., Vázquez-Olmos, A. R., Ortega-Maldonado, M., & Ximenez-Fyvie, L. A. (2023). Antibacterial properties in vitro of magnesium oxide nanoparticles for dental applications. *Nanomaterials*, *13*(3), 502.

[72] Wang, L., Hu, C., & Shao, L. (2017). The antimicrobial activity of nanoparticles: present situation and prospects for the future. *International journal of nanomedicine*, 1227-1249.

[73] Koper, O.B.; Klabunde, J.S.; Marchin, G.L.; Klabunde, K.J.; Stoimenov, P.; Bohra, L. Nanoscale Powders and Formulations with Biocidal Activity Toward Spores and Vegetative Cells of Bacillus Species, Viruses, and Toxins. *Curr. Microbiol.* **2002**, *44*, 49–55.

[74] Koper, O.B.; Lagadic, I.; Volodin, A.; Klabunde, K.J. Alkaline-Earth Oxide Nanoparticles Obtained by Aerogel Methods. Characterization and Rational for Unexpectedly High Surface Chemical Reactivities. *Chem. Mater.* **1997**, *9*, 2468–2480.

[75] Stoimenov, P.K.; Klinger, R.L.; Marchin, G.L.; Klabunde, K.J. Metal Oxide Nanoparticles as Bactericidal Agents. *Langmuir* **2002**, *18*, 6679–6686.

[76] Tang, Z.-X.; Lv, B.-F. MgO nanoparticles as antibacterial agent: Preparation and activity. *Braz. J. Chem. Eng.* **2014**, *31*, 591–601.

[77] Huang, L.; Li, D.-Q.; Lin, Y.-J.; Wei, M.; Evans, D.G.; Duan, X. Controllable preparation of Nano-MgO and investigation of its bactericidal properties. *J. Inorg. Biochem.* **2005**, *99*, 986–993.

[78] Yamamoto, O.; Sawai, J.; Sasamoto, T. Change in antibacterial characteristics with doping amount of ZnO in MgO–ZnO solid solution. *Int. J. Inorg. Mater.* **2000**, *2*, 451–454.

[79] Sambandam, T., Karuppasamy, G., Perumal, G., & Rajasingh, E. C. (2025). Liquid phase preparation and characterization of MgO nanoparticles and their butchery activities against dental bacterial pathogens and human cervical cancer cell line. *Journal of Photochemistry and Photobiology B: Biology*, *262*, 113084.

[80] Ulaş, F., Yüksel, E., Dinçer, D., Dababat, A., & İmren, M. (2025). Recent advances in plant-based green synthesis of nanoparticles: a sustainable approach for combating plant-parasitic nematodes. *Sustainability*, *17*(9), 4152.

[81] Abid, M. A., Kadhim, D. A., & Aziz, W. J. (2020). Iron oxide nanoparticle synthesis using trigonella and tomato extracts and their antibacterial activity. *Materials Technology*, *37*(8), 547–554. https://doi.org/10.1080/10667857.2020.1863572.

[82] Singh, H., Desimone, M. F., Pandya, S., Jasani, S., George, N., Adnan, M., ... & Alderhami, S. A. (2023). Revisiting the green synthesis of nanoparticles: uncovering influences of plant extracts as reducing agents for enhanced synthesis efficiency and its biomedical applications. *International journal of nanomedicine*, 4727-4750.

[83] Kadhim, D. A., Abid, M. A., & Salih, W. M. (2023). Study the degradation and photocatalytic activity of the methylene blue dye by mixing the Aloe vera extract with rust iron oxide nanoparticle.

[84] Kadhim, D. A., Raheem, A. H. A., Qasim, N., Abid, M. A., & Thabet, I. A. (2024). Development of a neutral resource for nano-AgO/Fe 2 O 3 composite preparation by mixing marine shrimp shell extract with metal salts for anti-microbial activity.